T-matrix approach to shale acoustics

Morten Jakobsen,[1] John A. Hudson[2] and Tor Arne Johansen[1]

[1] *University of Bergen, Department of Earth Science, Allegt.* 41, N-5007 *Bergen, Norway. E-mail: src@iffif.uib.no*
[2] *University of Cambridge, Department of Applied Mathematics and Theoretical Physics, Centre for Mathematical Sciences, Wilberforce Road, Cambridge*
CB3 0WA. *E-mail: J.A.Hudson@damtp.cam.ac.uk*

SUMMARY

The *T*-matrix approach of quantum scattering theory is used here to place many long-wavelength equivalent-medium approximations for porous composites, polycrystals and cracked media on a common footing and to indicate their limitations, but also to derive some new results based on two-point statistics. In this way, we have obtained an insight into the difficult problem of elastic inclusions at finite concentrations, which is of foremost relevance when estimating the effective material parameters of porous/cracked shales, involving stacks of more or less horizontally aligned clay platelets, mixed together with more rounded silt minerals, and with fluid filling the spaces. A rather involved perturbative analysis of the effects of interactions between (or structural correlations among) the various inclusions (minerals and cavities) making up a real shale of hexagonal symmetry was performed in an attempt to obtain a better match between theoretical predictions (based on a combination of coherent and optical potential approximations) and experimental results (recovered from ultrasonic wave speeds) for the effective elastic stiffness tensor. For the particular data set considered in this study, the *T*-matrix approach was able to match the data better than the approach of Hornby *et al.*, but the match was not completely satisfactory. Further progress in theoretical shale modelling may come from a better knowledge of the elastic properties of pure clay minerals, a more detailed knowledge of the microstructure of shales, the incorporation of constraints obtained from comparisons between theoretical predictions and experimental results, as well as a continuing development of the *T*-matrix approach. Numerical results (also for the effect of bedding parallel microcracks on the elasticity of such a real shale) have value in illustrating the importance of taking into account the effects of spatial distribution when trying to deal with non-dilute mixtures of highly contrasting material properties.

Key words: elastic composites, finite concentrations, mineralogy, seismic anisotropy.

1 INTRODUCTION

In the subdiscipline of rock physics called shale acoustics, the goal is to find out exactly what controls the behaviour of acoustic (infrasonic, sonic, ultrasonic) compressional and shear waves in one of nature's most abundant and complicated forms of matter. This is interesting both from an industrial perspective and from an academic one. Shales make up a major component of sedimentary basins and play an important role in fluid flow and wave propagation because of their low permeability and anisotropic microstructure. At all scales from ultrasonic to seismic (infrasonic/sonic), shales have been found to behave elastically as a transversely isotropic (TI) medium (e.g. Jakobsen & Johansen 1999, 2000). The five independent elastic parameters of a TI shale are often required as input to computer systems for seismic modelling and inversions. Since shales make up most of the overburden overlaying many of the world's hydrocarbon-bearing reservoirs, quantitative information concerning the velocity anisotropy of shales is typically needed for the calibration of amplitude versus offset (AVO) measurements (see Johansen *et al.* 2000, 2002a).

In the light of the manifest importance of determining the effective elastic constants of shales, a significant body of literature has evolved, based upon ultrasonic laboratory measurements (e.g. Kaarsberg 1959; Podio *et al.*1968; Jones & Wang 1981; Lo *et al.*1986; Johnston 1987; Yin 1993; Johnston & Christensen 1995; Hornby 1998; Jakobsen & Johansen 1999, 2000), seismic field measurements (White *et al.* 1983; Winterstein & Paulson 1990) and theoretical techniques (Hornby *et al.*1994; Sayers 1994, 1999; Jakobsen 1998; Hornby 2001; Johansen *et al.* 2002). Nevertheless, our understanding of the scaling problems associated with wave propagation in shale formations is still not adequate (e.g. Thomsen 1986; Vernik & Liu 1997; Hornby 2001). In the paper of Hornby (2001) it is written that 'comparison of intrinsic anisotropy

of shales measured on whole core at ultrasonic frequencies in the laboratory with seismic scale anisotropy estimated using walkaway VSP surveys reveal systematic differences that are attributed to fine layer effects'. The goal of this study is to present a method to predict the core-scale intrinsic anisotropy of (cracked) shales from the parameters of the microstructures. The methods we are developing can, however, also lead to a better understanding of the up-scaling problem in finely layered anisotropic media (see Dederich & Zeller 1972, Chapter 8).

Under a microscope (fig. 1 in the paper by Hornby *et al.* 1994; Bennett *et al.* 1991), shales typically appear as stacks of more or less horizontally aligned clay platelets, mixed together with more rounded silt minerals, and with fluid and perhaps cements filling the spaces. Like all other rocks, shales may also contain microscopic cracks that dramatically affect their overall properties, even when the volume concentration of cracks is very small. Little work has been done on the effects of cracks in shale acoustics, although Vernik (1994) has suggested that bedding parallel microcracks may exist *in situ* in most mature source shales undergoing the major stage of hydrocarbon generation and migration. It is clear that cracks in shales may not only be created during such (and other) natural processes, but also during 'artificial' processes, associated with operations such as drilling, core taking and sample preparation. For a variety of reasons, it is therefore important to be able to separate the crack-induced anisotropy of a shale from the anisotropy associated with other alignments in the microstructure. The present study may help to make sense of it all.

Any theory for the macroscopic properties of (cracked) shales needs to have a strong stochastic component, since randomness is one of the most prominent features of these materials. With the introduction of a general model for anisotropic media with inclusions or cavities, the computation of the effective elastic parameters of (cracked) shales becomes a many-body problem similar to the one that has been studied in modern physics for the last 40 years or so. It was therefore natural for us to look in the quantum mechanical literature (e.g. Watson 1957; Goldberger & Watson 1964; Soven 1967; Taylor 1967; March *et al.*1967; Elliott *et al.*1974) to find inspiration for solving the many-body problem in shale acoustics. With the introduction of formal perturbation techniques in this classical part of physics, we hope to clarify discussions concerning different modelling strategies for materials that are heterogeneous at multiple scales.

The three-step modelling procedure for (uncracked) shales introduced by Hornby *et al.* (1994) is based on a combination of simple volume averaging (Hudson 1991), the method of eigenstrain (see Mura 1982) and intuitive arguments that do not allow for an explicit description of the interaction between (or structural correlations among) the inclusions. If the concentrations of inclusions are small then it is possible to describe such interaction effects explicitly using the method of smoothing (see Keller 1964). This was demonstrated by Hudson (1994b) in his study of the elasticity of a cracked anisotropic solid. It can be expected that such interaction effects become large when the concentrations are no longer small.

In an attempt to solve the difficult problem of elastic inclusions at finite concentrations, we decided to employ the very powerful *T*-matrix approach of quantum scattering theory, which has already enjoyed great success outside rock physics. Since Zeller & Dederichs (1973) first used the *T*-matrix approach to estimate the effective elastic constants of a disordered solid, this method has received a lot of attention (see Nan *et al.* 1998) but, despite many efforts, the interaction between different inclusions (that are not necessarily spherical and embedded in an isotropic matrix material) has hitherto not been explicitly described in the *T*-matrix language. This situation has now changed, in the sense that we have not only managed to place many effective medium theories of porous composites, polycrystals and cracked media on a common footing and indicate their limitations, but also obtained some new results based on two-point statistics.

All of these comments have hopefully motivated the reader for a 'grand unified tour' of theoretical shale acoustics. We shall start with five rather theoretical sections dealing with the *T*-matrix approach itself. We shall then proceed with a more computational oriented section, focusing on the averaging of fourth-rank tensors using texture or crystal orientation distribution functions (ODFs). The overall idea is to create a perturbative atmosphere for the subsequent section called 'Shale acoustics from a modern perspective', where we fit ultrasonic measurements and predict the effects of cracks in shales. Before we start, let us note that the effective stiffnesses provided by our static theory of composites, and the mean density for the heterogeneous material as a whole, represents all the parameters we need to predict the most probable behaviour of the mean wave propagating in a random composite such as a shale, provided that wavelengths are relatively long compared with the size of a representative volume element containing a large number of inclusions. We refer to the work of Willis (1981) for discussions concerning the effective behaviour of waves in composites in this so-called Rayleigh limit.

2 DEFINITIONS AND FUNDAMENTAL EQUATIONS

We assume that an elastic specimen with complex microstructure occupies a large spherical region Ω. Under a deformation with infinitesimal strain, the stress tensor $\boldsymbol{\sigma}(\mathbf{x})$ and strain tensor $\boldsymbol{\epsilon}(\mathbf{x})$ at point $\mathbf{x}$ are related by the linear transformation

$$\boldsymbol{\sigma}(\mathbf{x}) = \boldsymbol{C}(\mathbf{x})\boldsymbol{\epsilon}(\mathbf{x}), \tag{1}$$

where $\boldsymbol{C}(\mathbf{x})$ is the local tensor of elastic constants. The complex microstructure of the specimen is reflected in the fact that $\boldsymbol{C}(\mathbf{x})$ varies with $\mathbf{x}$ in a random manner, on a scale that is small compared with all other length-scales; e.g. the size of the specimen and the wavelength of an acoustic wave. If a similar relation holds for the heterogeneous material as a whole, namely in terms of the averaged stress tensor $\langle\boldsymbol{\sigma}(\mathbf{x})\rangle$ and strain tensor $\langle\boldsymbol{\epsilon}(\mathbf{x})\rangle$,

$$\langle\boldsymbol{\sigma}(\mathbf{x})\rangle = \boldsymbol{C}^*\langle\boldsymbol{\epsilon}(\mathbf{x})\rangle, \tag{2}$$

then our problem is to determine the tensor $\boldsymbol{C}^*$ of effective elastic constants using the statistical information we have about $\boldsymbol{C}(\mathbf{x})$. In eq. (2) the angular brackets $\langle\cdot\rangle$ denote the ensemble average, which may be replaced by the volume average if the material is statistically homogeneous.

By statistical homogeneity we mean that any sufficiently large (compared to the scale of the microstructure) subregion of Ω is statistically identical to the whole specimen. If the material is statistically homogeneous, as we assume in the following, all ensemble-averaged material quantities, such as $\boldsymbol{C}^*$, are independent of position.

Eq. (2) represents the use of a local constitutive relation at the macroscopic level. More generally, we could have related the ensemble-averaged stress and strain fields by a non-local integral operator (see Zeller & Dederichs 1973), but since the non-locality of the overall elastic properties of a heterogeneous material is typically restricted to a small correlation length, we decided to ignore this phenomenon. We may therefore avoid the rather abstract operator notation of Zeller & Dederichs (1973).

To evaluate the tensor of effective elastic constants from eq. (2), we begin by introducing an integral equation for the strain tensor field

$$\epsilon(\mathbf{x}) = \frac{1}{2}\left\{\nabla\mathbf{u}(\mathbf{x}) + [\nabla\mathbf{u}(\mathbf{x})]^{\mathrm{T}}\right\}, \tag{3}$$

under a known displacement $\mathbf{u}(\mathbf{x})$ of the surface $\partial\Omega$ of the specimen Ω:

$$\mathbf{u}(\mathbf{x}) = \mathbf{U}(\mathbf{x}), \quad \mathbf{x} \in \partial\Omega. \tag{4}$$

We start with the equilibrium equation

$$\nabla \cdot \boldsymbol{\sigma}(\mathbf{x}) = 0. \tag{5}$$

Since the material is homogeneous on the macroscopic scale, it makes sense to write

$$\boldsymbol{C}(\mathbf{x}) = \boldsymbol{C}^{(0)} + \delta\boldsymbol{C}(\mathbf{x}), \tag{6}$$

where $\delta\boldsymbol{C}(\mathbf{x})$ is the fluctuation of $\boldsymbol{C}(\mathbf{x})$ from a quantity $\boldsymbol{C}^{(0)}$, which is uniform in space. The choice of $\boldsymbol{C}^{(0)}$ may be rather arbitrary but is subjected to the constraint that the mechanical stability criterion (all principal minors of $\det\boldsymbol{C}^{(0)}$ must be positive) is not violated (see Auld 1990; Sarkar *et al.* 1996). It follows from eqs (1), (5) and (6) that

$$\nabla \cdot \left[\boldsymbol{C}^{(0)}\epsilon(\mathbf{x})\right] = -\nabla \cdot [\delta\boldsymbol{C}(\mathbf{x})\epsilon(\mathbf{x})], \tag{7}$$

where the term on the right-hand side may formally be regarded as an applied force density.

An integral equation for the strain field may now be derived from the complicated differential equation (7) (see Zeller & Dederichs 1973; Gubernatis & Krumhansl 1975; Willis 1981);

$$\epsilon(\mathbf{x}) = \epsilon^{(0)} + \int_\Omega d\mathbf{x}' \boldsymbol{G}^{(0)}(\mathbf{x} - \mathbf{x}')\delta\boldsymbol{C}(\mathbf{x}')\epsilon(\mathbf{x}'), \tag{8}$$

where $\epsilon^{(0)}$ is the strain tensor due to the boundary displacements in a material with properties given by $\boldsymbol{C}^{(0)}$. In eq. (8) we have introduced the strain Green's tensor function $\boldsymbol{G}^{(0)}(\mathbf{x})$ for a translation-invariant system, for which the components are given by

$$G^{(0)}_{ijkl}(\mathbf{x}) = -\frac{1}{4}\left[\frac{g^{(0)}_{ik}(\mathbf{x})}{\partial x_j \partial x_l} + \frac{g^{(0)}_{jk}(\mathbf{x})}{\partial x_i \partial x_l} + \frac{g^{(0)}_{il}(\mathbf{x})}{\partial x_j \partial x_k} + \frac{g^{(0)}_{jl}(\mathbf{x})}{\partial x_i \partial x_k}\right], \tag{9}$$

where $g^{(0)}_{ik}(\mathbf{x})$ is a component of the displacement Green's tensor function $\mathbf{g}^{(0)}(\mathbf{x})$, which vanishes at the boundary of Ω:

$$C^{(0)}_{ijkl}\frac{\partial^2 g^{(0)}_{km}(\mathbf{x})}{\partial x_j \partial x_l} + \delta_{im}\delta(\mathbf{x}) = 0, \quad \mathbf{g}^{(0)}(\mathbf{x}) = 0 \quad \text{if} \quad \mathbf{x} \in \partial\Omega. \tag{10}$$

Let us note that the functions $\mathbf{g}^{(0)}(\mathbf{x})$ and $\boldsymbol{G}^{(0)}(\mathbf{x})$ have simple physical interpretations: for a homogeneous medium with tensor of elastic constants $\boldsymbol{C}^{(0)}$, $g^{(0)}_{ij}(\mathbf{x} - \mathbf{x}')$ is the displacement in the ith direction at $\mathbf{x}$ due to a point force applied in the jth direction at $\mathbf{x}'$. Correspondingly, $G^{(0)}_{ijkl}(\mathbf{x} - \mathbf{x}')$ is the ij strain at $\mathbf{x}$ due to a kl stress (dipole) at $\mathbf{x}'$. According to Gubernatis & Krumhansl (1975), $\delta\boldsymbol{C}(\mathbf{x}')$ 'scatters' the strain field from $\mathbf{x}'$ to $\mathbf{x}$ via the 'propagator' $\boldsymbol{G}^{(0)}(\mathbf{x} - \mathbf{x}')$. The singularity of the strain Green's function at the origin should be interpreted in the sense of distributions (see Willis 1977; Kroner 1986).

The integral equation (8) is similar to the Lippmann–Schwinger (or Dyson) equation in quantum scattering theory (e.g. March *et al.* 1967; Goldberger & Watson 1969; Elliott *et al.* 1974; Kroner 1986). This is an agreeable feature because it permits us to use the highly developed perturbative or iterative methods developed in that part of physics. Following Zeller & Dederichs (1973), we now introduce a fourth-rank tensor field $\boldsymbol{T}(\mathbf{x})$ which, when contracted with $\epsilon^{(0)}$ on the right, yields the stress difference $\delta\boldsymbol{C}(\mathbf{x})\epsilon(\mathbf{x})$; that is,

$$\delta\boldsymbol{C}(\mathbf{x})\epsilon(\mathbf{x}) = \boldsymbol{T}(\mathbf{x})\epsilon^{(0)}. \tag{11}$$

Since this is a linear problem, $\epsilon(\mathbf{x})$ is linearly dependent on $\epsilon^{(0)}$ through the boundary condition (eq. 4) and so $\boldsymbol{T}(\mathbf{x})$ depends only on the material properties and not on $\epsilon(\mathbf{x})$ or $\epsilon^{(0)}$. We now proceed to find an integral equation, similar to eq. (8), for $\boldsymbol{T}(\mathbf{x})$. Using eq. (11) in eq. (8) we obtain

$$\epsilon(\mathbf{x}) = \epsilon^{(0)} + \int_\Omega d\mathbf{x}' \boldsymbol{G}^{(0)}(\mathbf{x} - \mathbf{x}')\boldsymbol{T}(\mathbf{x}')\epsilon^{(0)}. \tag{12}$$

By multiplying eq. (12) with $\delta\boldsymbol{C}(\mathbf{x})$ from the left and using eq. (11) again, we obtain

$$\boldsymbol{T}(\mathbf{x})\epsilon^{(0)} = \delta\boldsymbol{C}(\mathbf{x})\epsilon^{(0)} + \delta\boldsymbol{C}(\mathbf{x})\int_\Omega d\mathbf{x}' \boldsymbol{G}^{(0)}(\mathbf{x} - \mathbf{x}')\boldsymbol{T}(\mathbf{x}')\epsilon^{(0)}. \tag{13}$$

We may choose the elements T_{ijkl} of $\boldsymbol{T}$ to be symmetric in (i, j) and (k, l) and, since $\epsilon^{(0)}$ may be chosen to be an arbitrary symmetric matrix,

it follows that

$$T(\mathbf{x}) = \delta C(\mathbf{x}) + \delta C(\mathbf{x}) \int_{\Omega} d\mathbf{x}' G^{(0)}(\mathbf{x} - \mathbf{x}') T(\mathbf{x}'). \tag{14}$$

The non-local counterpart of eq. (14) was first presented in an operator notation by Zeller & Dederichs (1973). The tensor field $T(\mathbf{x})$ specifies the 'transitions' out of the reference field $\epsilon^{(0)}$ and give us complete information concerning the strain tensor field distribution $\epsilon(\mathbf{x})$ in the microinhomogeneous material, provided that we can solve the integral eq. (14). In the following we shall refer to $T(\mathbf{x})$ as the T-matrix for the material.

To complete this section, let us evaluate the tensor of effective elastic constants in terms of T. From eqs (1) and (6), we obtain

$$\langle \boldsymbol{\sigma} \rangle = C^{(0)} \langle \epsilon \rangle + \langle \delta C \epsilon \rangle. \tag{15}$$

By combining eqs (11) and (15) we obtain

$$\langle \boldsymbol{\sigma} \rangle = C^{(0)} \langle \epsilon \rangle + \langle T \rangle \epsilon^{(0)}. \tag{16}$$

From eq. (12) it is clear that

$$\langle \epsilon \rangle = \epsilon^{(0)} + \bar{G} \langle T \rangle \epsilon^{(0)}, \tag{17}$$

where

$$\bar{G} = \int_{\Omega} d\mathbf{x}' G^{(0)}(\mathbf{x} - \mathbf{x}'), \quad \mathbf{x} \in \Omega, \tag{18}$$

is a constant tensor (see Eshelby 1957; Willis 1977; Mura 1982; Kroner 1986). Eq. (17) gives $\epsilon^{(0)}$ in terms of $\langle \epsilon \rangle$:

$$\epsilon^{(0)} = (I + \bar{G} \langle T \rangle)^{-1} \langle \epsilon \rangle, \tag{19}$$

where the components of the (identity) tensor I are given by

$$I_{ijkl} = \frac{1}{2}(\delta_{ik}\delta_{jl} + \delta_{il}\delta_{jk}). \tag{20}$$

Eqs (2), (16) and (19), imply that

$$C^* = C^{(0)} + \langle T \rangle (I + \bar{G} \langle T \rangle)^{-1}. \tag{21}$$

Thus we have actually obtained a formal exact solution for the practical interesting case of local elasticity, given earlier by Zeller & Dederichs (1973) for the more obscure case of non-local elasticity, in terms of the (yet to be determined) T-matrix for the material. For convenience of calculation, we have assumed that a state of homogeneous strain has been set up by choosing a spherical shape and suitable boundary conditions for the macroscopic specimen. Our intermediate results may depend on these special conditions, but not the final results (see McCoy 1979). The effective elastic constants are material properties and do not depend on the shape of the test specimen or the stress/strain in the system.

3 INCLUSION-BASED MODELS

Whereas all previous equations are valid for the tensor of elastic constants $C(\mathbf{x})$ arbitrarily varying in space, we restrict ourselves now to materials in which $C(\mathbf{x})$ is piecewise constant. Specifically, we consider media with inclusions that are either embedded in a homogeneous matrix material or else make up a granular aggregate. The inclusions we are dealing with may have any shape and orientation. Our goal is to develop a 'unified' theory to predict the macroscopic properties of microinhomogeneous media (including porous composites, polycrystals, and cracked media) from the parameters of the microstructure. The population of inclusions is divided into families of inclusions having the same shape/orientation and stiffness tensor $C^{(r)}$, labelled by $r = 1, 2, \ldots, F$. Dry cavities may formally be treated as inclusions having vanishing stiffnesses (see Nemat-Nasser & Hori 1993; Ponte Castaneda & Willis 1995). We assume that there are $n^{(r)}$ inclusions of type r, occupying identical regions $\Omega_{\alpha}^{(r)}$ of the space Ω, centred at random points $\mathbf{x}_{\alpha}^{(r)}$ ($\alpha = 1, \ldots, n^{(r)}$). Denote by $\theta^{(r)}(\mathbf{x})$ the characteristic function of the domain $\Omega_{\alpha}^{(r)}$ (that is, $\theta^{(r)}(\mathbf{x} - \mathbf{x}_{\alpha}^{(r)}) = 1$, if $\mathbf{x} \in \Omega_{\alpha}^{(r)}$ and 0 otherwise); it follows that the fluctuation $\delta C(\mathbf{x})$ may be decomposed as

$$\delta C(\mathbf{x}) = \sum_{r=1}^{F} \sum_{\alpha=1}^{n^{(r)}} \delta C_{\alpha}^{(r)}(\mathbf{x}), \tag{22}$$

$$\delta C_{\alpha}^{(r)}(\mathbf{x}) = \delta C^{(r)} \theta^{(r)}(\mathbf{x} - \mathbf{x}_{\alpha}^{(r)}), \tag{23}$$

$$\delta C^{(r)} = C^{(r)} - C^{(0)}. \tag{24}$$

A decomposition of the T-matrix for the material, which is analogous with that of $\delta C(\mathbf{x})$ in eq. (22), is given by

$$T(\mathbf{x}) = \sum_{r=1}^{F} \sum_{\alpha=1}^{n^{(r)}} T_{\alpha}^{(r)}(\mathbf{x}), \tag{25}$$

$$T_{\alpha}^{(r)}(\mathbf{x}) = T(\mathbf{x}) \theta^{(r)}(\mathbf{x} - \mathbf{x}_{\alpha}^{(r)}). \tag{26}$$

Eqs (14), (22) and (25), imply that the $\boldsymbol{T}'^{(r)}_\alpha(\mathbf{x})$ must satisfy

$$\boldsymbol{T}'^{(r)}_\alpha(\mathbf{x}) = \delta\boldsymbol{C}^{(r)}_\alpha(\mathbf{x}) + \delta\boldsymbol{C}^{(r)}_\alpha(\mathbf{x}) \int_\Omega d\mathbf{x}' \boldsymbol{G}^{(0)}(\mathbf{x} - \mathbf{x}') \sum_{s,\beta} \boldsymbol{T}^{(s)}_\beta(\mathbf{x}'). \tag{27}$$

In Appendix A it is shown that, if we let $\boldsymbol{t}^{(r)}_\alpha(\mathbf{x})$ denote the solution of the integral equation (eq. A7):

$$\boldsymbol{t}^{(r)}_\alpha(\mathbf{x}) = \delta\boldsymbol{C}^{(r)}_\alpha(\mathbf{x}) + \delta\boldsymbol{C}^{(r)}_\alpha(\mathbf{x}) \int_\Omega d\mathbf{x}' \boldsymbol{G}^{(0)}(\mathbf{x} - \mathbf{x}') \boldsymbol{t}^{(r)}_\alpha(\mathbf{x}'), \tag{28}$$

then we may rewrite expression (27) for $\boldsymbol{T}'^r_\alpha(\mathbf{x})$ exactly as (eq. A5)

$$\boldsymbol{T}^{(r)}_\alpha(\mathbf{x}) = \boldsymbol{t}^{(r)}_\alpha(\mathbf{x}) + \boldsymbol{t}^{(r)}_\alpha(\mathbf{x}) \int_\Omega d\mathbf{x}' \boldsymbol{G}^{(0)}(\mathbf{x} - \mathbf{x}') \sum_{s,\beta} \boldsymbol{T}^{(s)}_\beta(\mathbf{x}')(1 - \delta_{rs}\delta_{\alpha\beta}), \tag{29}$$

which has the form of the central equation that describe the multiple scattering of waves in a typical many-body system (see Korringa 1979). Comparison between eqs (14) and (28) shows that $\boldsymbol{t}^{(r)}_\alpha(\mathbf{x})$ is the t-matrix for a medium with stiffness fluctuation $\delta\boldsymbol{C}(\mathbf{x}) = \delta\boldsymbol{C}^{(r)}_\alpha(\mathbf{x})$. This means that, for a medium with a single inclusion of type r at $\mathbf{x} = \mathbf{x}^{(r)}_\alpha$ embedded in a uniform matrix with properties given by $\boldsymbol{C}^{(0)}$, the t-matrix $\boldsymbol{t}^{(r)}_\alpha(\mathbf{x})$ gives us the strain inside the inclusion (r, α) by the use of eq. (11), and at an arbitrary point by the use of eq. (8). We may therefore say that $\boldsymbol{t}^{(r)}_\alpha(\mathbf{x})$ completely solves the single-body problem. The second term on the right-hand side of eq. (29) obviously describes the interaction of different bodies or inclusions.

Successive iterations of eq. (29) will lead to a cluster expansion similar to those developed in quantum mechanics (see March *et al.* 1967; Goldberger & Watson 1964; Elliott *et al.* 1974). In principle our theory can deal with clusters involving any number of bodies. However, the calculations quickly become very difficult if we go beyond the two-body problem. Therefore, we shall restrict ourselves to approximations involving clusters of two bodies based on two-point statistics. A single iteration of eq. (29) yields

$$\boldsymbol{T}^{(r)}_\alpha(\mathbf{x}) \approx \boldsymbol{t}^{(r)}_\alpha(\mathbf{x}) + \boldsymbol{t}^{(r)}_\alpha(\mathbf{x}) \int_\Omega d\mathbf{x}' \boldsymbol{G}^{(0)}(\mathbf{x} - \mathbf{x}') \sum_{s,\beta} \boldsymbol{t}^{(s)}_\beta(\mathbf{x}')(1 - \delta_{rs}\delta_{\alpha\beta}). \tag{30}$$

Since $\boldsymbol{C}^{(0)}$ is rather arbitrary, its value can sometimes be chosen so that even the single inclusion transition tensor $\boldsymbol{t}^{(r)}_\alpha(\mathbf{x})$ takes into account the interaction between different inclusions to some degree (see Soven 1967; Taylor 1967). One the other hand, the second term on the right-hand side of eq. (30) is directly related to interactions between two inclusions only.

4 THE T-MATRIX FOR A SINGLE INCLUSION

A single homogeneous inclusion embedded in a homogeneous matrix subjected to homogeneous strain at infinity undergoes a deformation which, if the inclusion is ellipsoidal in shape, also corresponds to a uniform internal strain field (Eshelby 1957; Mura 1982; Kroner 1986). We now assume that the inclusions we are dealing with are ellipsoidal in shape or, if they are not, then to take the internal strain field, in the circumstances described above, to be constant will lead to a good approximation. If the material consists of inclusions embedded in a homogeneous matrix, we should take $\boldsymbol{C}^{(0)}$ to correspond to the properties of the matrix. It then follows from eq. (28) that $\boldsymbol{t}^{(r)}_\alpha(\mathbf{x})$ for the matrix is zero. If we do not take this step, we would need to calculate $\boldsymbol{t}^{(r)}_\alpha(\mathbf{x})$ for the matrix, which definitely cannot be approximated in shape by an ellipsoid.

The transition tensor $\boldsymbol{t}^{(r)}_\alpha(\mathbf{x})$ satisfies (see eq. 11)

$$\delta\boldsymbol{C}^{(r)}_\alpha(\mathbf{x})\boldsymbol{\epsilon}^{(r)}_\alpha(\mathbf{x}) = \boldsymbol{t}^{(r)}_\alpha(\mathbf{x})\boldsymbol{\epsilon}^{(0)}, \tag{31}$$

where $\boldsymbol{\epsilon}^{(r)}_\alpha(\mathbf{x})$ is the strain field for a single inclusion of type r embedded in the homogeneous matrix. If $\boldsymbol{\epsilon}^{(r)}_\alpha(\mathbf{x})$ is constant within the inclusion, then $\boldsymbol{t}^{(r)}_\alpha(\mathbf{x})$ must also be; and it is zero outside, so we may write

$$\boldsymbol{t}^{(r)}_\alpha(\mathbf{x}) = \boldsymbol{t}^{(r)}\theta^{(r)}\left(\mathbf{x} - \mathbf{x}^{(r)}_\alpha\right), \tag{32}$$

where $\boldsymbol{t}^{(r)}$ is a constant tensor. Inserting this into the integral eq. (28), we obtain

$$\boldsymbol{t}^{(r)}\theta^{(r)}\left(\mathbf{x} - \mathbf{x}^{(r)}_\alpha\right) = \delta\boldsymbol{C}^{(r)}\theta^{(r)}\left(\mathbf{x} - \mathbf{x}^{(r)}_\alpha\right) + \delta\boldsymbol{C}^{(r)}\theta^{(r)}\left(\mathbf{x} - \mathbf{x}^{(r)}_\alpha\right) \int_\Omega d\mathbf{x}' \boldsymbol{G}^{(0)}(\mathbf{x} - \mathbf{x}')\boldsymbol{t}^{(r)}\theta^{(r)}\left(\mathbf{x}' - \mathbf{x}^{(r)}_\alpha\right). \tag{33}$$

We now integrate over Ω to obtain

$$\boldsymbol{t}^{(r)} = \delta\boldsymbol{C}^{(r)} + \delta\boldsymbol{C}^{(r)}\boldsymbol{G}^{(r)}\boldsymbol{t}^{(r)}, \tag{34}$$

or

$$\boldsymbol{t}^{(r)} = \left(\boldsymbol{I} - \delta\boldsymbol{C}^{(r)}\boldsymbol{G}^{(r)}\right)^{-1}\delta\boldsymbol{C}^{(r)}, \tag{35}$$

where

$$\boldsymbol{G}^{(r)} = \frac{1}{\left|\Omega^{(r)}\right|} \int_{\Omega^{(r)}} d\mathbf{x} \int_{\Omega^{(r)}} d\mathbf{x}' \boldsymbol{G}^{(0)}(\mathbf{x} - \mathbf{x}'), \tag{36}$$

and $\Omega^{(r)}$ is the region of an inclusion of type r centred at the origin. Clearly, $\boldsymbol{G}^{(r)}$ is a constant tensor, and its components can be evaluated using the formulae discussed below. Thus, we have a means of calculating $\boldsymbol{t}^{(r)}$ and hence $\boldsymbol{t}^{(r)}_\alpha(\mathbf{x})$.

From the work of Kroner (1986) it is clear that

$$G^{(r)}_{pqrs} = -\frac{1}{4}\left[E^{(r)}_{pqrs} + E^{(r)}_{pqsr} + E^{(r)}_{qprs} + E^{(r)}_{qpsr}\right], \tag{37}$$

where

$$E^{(r)}_{pqrs} = \int_0^\pi d\theta \sin\theta \int_0^{2\pi} d\phi\, D^{-1}_{qs}(\mathbf{k})k_p k_r A^{(r)}(\theta,\phi), \tag{38}$$

and $D^{-1}_{pr}(\mathbf{k})$ is the inverse matrix of the Fourier transform of the displacement Green's function, and

$$A^{(r)}(\theta,\phi) = \frac{1}{\pi\left|\Omega^{(r)}\right|}\int_0^\infty dk k^2 \int_{\Omega^{(r)}} d\mathbf{x} e^{-i\mathbf{k}\cdot\mathbf{x}}\int_{\Omega^{(r)}} d\mathbf{x}' e^{i\mathbf{k}\cdot\mathbf{x}'}, \tag{39}$$

where k, θ and ϕ are spherical coordinates in $\mathbf{k}$ space, and k_i are the Cartesian components of $\mathbf{k}$. Obviously, $A^{(r)}$ represents a shape/orientation factor independent of the elastic constants. For a sphere, $A^{(r)} = 1/(4\pi)$, and so $\boldsymbol{G}^{(r)}$ is actually independent of the orientation/shape index r in this case. For an ellipsoid, things become more complicated. To illustrate this, let us assume $\Omega^{(r)}$ represents an oblate spheroid with short axis b_3 parallel to the Ox_3 direction (and long axis $b_2 = b_1$), so that, for $\mathbf{k} \neq 0$, then (see Nemat-Nasser & Hori 1993)

$$\int_{\Omega^{(r)}} d\mathbf{x}\exp(i\mathbf{k}\cdot\mathbf{x}) = \frac{3|\Omega^{(r)}|}{\eta^3}(\sin\eta - \eta\cos\eta), \tag{40}$$

where

$$\eta = \left[(k_1 b_1)^2 + (k_2 b_1)^2 + (k_3 b_3)^2\right]^{1/2}. \tag{41}$$

With

$$\mathbf{k} = k[\sin\theta\cos\phi, \sin\theta\sin\phi, \cos\theta], \tag{42}$$

we can write

$$\eta = ak, \quad a = \left[b_1^2\sin^2\theta + b_3^2\cos^2\theta\right]^{1/2}. \tag{43}$$

Since we have assumed the shape of $\Omega^{(r)}$ to be essentially 2-D, it is not surprising that ϕ has disappeared from our equations. The integral $\int_{\Omega^{(r)}}\exp(-i\mathbf{k}\cdot\mathbf{x}')\,d\mathbf{x}'$ yields the same result, and from eq. (39) we have

$$A^{(r)} = \frac{(3|\Omega^{(r)}|)^2}{8\pi^3|\Omega^{(r)}|a^6}\int_0^\infty dk k^2 \frac{(\sin ak - ak\cos ak)^2}{k^6}. \tag{44}$$

From Morris (1970) it is clear that

$$\int_0^\infty dk \frac{(\sin ak - ak\cos ak)^2}{k^4} = \frac{\pi a^3}{6}. \tag{45}$$

Hence, with $|\Omega^{(r)}| = \frac{4}{3}\pi b_1^2 b_3$, the purely geometric factor $A^{(r)}$ reduces to

$$A^{(r)}(\theta) = \frac{1}{4\pi}\frac{b_1^2 b_3}{\left(b_1^2\sin^2\theta + b_3^2\cos^2\theta\right)^{3/2}}. \tag{46}$$

Further progress along this line may now easily be obtained by first combining eqs (38) and (46) and then solve the resulting integrals using symbolic and/or numerical methods. For other treatments and, partially, more general theorems of the inclusion problem, see Mura (1982),

Ponte Castaneda & Willis (1995) and Kroner (1986, p. 262). Surprisingly enough, we have not seen the rather elementary derivations in this last paragraph on paper before.

5 THE T-MATRIX FOR A COMPOSITE MATERIAL

After some trivial manipulations, we find from eqs (25), (30) and (32), that

$$\boldsymbol{T}(\mathbf{x}) \approx \boldsymbol{T}_1(\mathbf{x}) + \boldsymbol{T}_2(\mathbf{x}), \tag{47}$$

where

$$\boldsymbol{T}_1(\mathbf{x}) = \sum_r \boldsymbol{t}^{(r)} \bar{\theta}^{(r)}(\mathbf{x}), \tag{48}$$

$$\boldsymbol{T}_2(\mathbf{x}) = \sum_r \sum_s \boldsymbol{t}^{(r)} \int_\Omega d\mathbf{x}' \boldsymbol{G}^{(0)}(\mathbf{x} - \mathbf{x}') \bar{\theta}^{(r)}(\mathbf{x}) \bar{\theta}^{(s)}(\mathbf{x}') \boldsymbol{t}^{(s)} - \sum_{r,\alpha} \boldsymbol{t}^{(r)} \theta^{(r)} \left(\mathbf{x} - \mathbf{x}_\alpha^{(r)} \right) \int_\Omega d\mathbf{x}' \boldsymbol{G}^{(0)}(\mathbf{x} - \mathbf{x}') \theta^{(r)} \left(\mathbf{x}' - \mathbf{x}_\alpha^{(r)} \right) \boldsymbol{t}^{(r)}, \tag{49}$$

and

$$\bar{\theta}^{(r)}(\mathbf{x}) = \sum_\alpha \theta^{(r)} \left(\mathbf{x} - \mathbf{x}_\alpha^{(r)} \right), \tag{50}$$

is the indicator function for phase r.

In order to evaluate the effective elastic constants from eq. (21), or from some equation implied by it, we need to construct an equivalent $\langle \boldsymbol{T} \rangle$. From eq. (47) we obtain

$$\langle \boldsymbol{T} \rangle \approx \langle \boldsymbol{T}_1 \rangle + \langle \boldsymbol{T}_2 \rangle. \tag{51}$$

Eq. (48) yields

$$\langle \boldsymbol{T}_1 \rangle = \sum_r \boldsymbol{t}^{(r)} v^{(r)}, \tag{52}$$

where

$$v^{(r)} = \left\langle \bar{\theta}^{(r)}(\mathbf{x}) \right\rangle, \tag{53}$$

is the relative volume concentration of phase r. From eq. (49) we obtain

$$\langle \boldsymbol{T}_2 \rangle = \sum_r \sum_s \boldsymbol{t}^{(r)} \int_\Omega d\mathbf{x}' \boldsymbol{G}^{(0)}(\mathbf{x} - \mathbf{x}') \left\langle \bar{\theta}^{(r)}(\mathbf{x}) \bar{\theta}^{(s)}(\mathbf{x}') \right\rangle \boldsymbol{t}^{(s)} - \sum_r \boldsymbol{t}^{(r)} \tilde{\boldsymbol{G}}^{(r)} \boldsymbol{t}^{(r)}, \tag{54}$$

where

$$\tilde{\boldsymbol{G}}^{(r)} = \sum_\alpha \frac{1}{|\Omega|} \int_\Omega d\mathbf{x} \theta^{(r)} (\mathbf{x} - \mathbf{x}_\alpha^{(r)}) \int_\Omega d\mathbf{x}' \boldsymbol{G}^{(0)}(\mathbf{x} - \mathbf{x}') \theta^{(r)} \left(\mathbf{x}' - \mathbf{x}_\alpha^{(r)} \right), \tag{55}$$

and we have replaced the ensemble average of the second term on the right-hand side of eq. (49) by its volume average. Eqs (36) and (55) imply that

$$\tilde{\boldsymbol{G}}^{(r)} = v^{(r)} \boldsymbol{G}^{(r)}, \tag{56}$$

since

$$v^{(r)} = \sum_\alpha \frac{\left| \Omega^{(r)} \right|}{|\Omega|} = n^{(r)} \frac{\left| \Omega^{(r)} \right|}{|\Omega|}. \tag{57}$$

6 THE EFFECTIVE ELASTIC CONSTANTS

The exact expression (21) for $\boldsymbol{C}^*$ can be rewritten exactly (as implicitly suggested by Torquato 1998; Nan *et al.* 1998)

$$(\delta \boldsymbol{C}^*)^{-1} = \langle \boldsymbol{T} \rangle^{-1} + \bar{\boldsymbol{G}}, \tag{58}$$

where

$$\delta \boldsymbol{C}^* = \boldsymbol{C}^* - \boldsymbol{C}^{(0)}. \tag{59}$$

Multiplying eq. (58) with $\langle \boldsymbol{T}_1 \rangle$ from the left and using the standard rule for inversion of tensor inner products, we obtain

$$\langle \boldsymbol{T}_1 \rangle (\delta \boldsymbol{C}^*)^{-1} = \left[\langle \boldsymbol{T} \rangle \langle \boldsymbol{T}_1 \rangle^{-1} \right]^{-1} + \langle \boldsymbol{T}_1 \rangle \bar{\boldsymbol{G}}. \tag{60}$$

Combining eqs (51) and (60), we obtain

$$\langle \boldsymbol{T}_1 \rangle (\delta \boldsymbol{C}^*)^{-1} \approx \left[\boldsymbol{I} + \langle \boldsymbol{T}_2 \rangle \langle \boldsymbol{T}_1 \rangle^{-1} \right]^{-1} + \langle \boldsymbol{T}_1 \rangle \bar{\boldsymbol{G}}. \tag{61}$$

If we now assume that

$$\left\| \langle \boldsymbol{T}_2 \rangle \langle \boldsymbol{T}_1 \rangle^{-1} \right\| < 1, \tag{62}$$

where $\| \cdot \|$ denotes a suitable tensor norm, then it follows from eq. (61) that $\delta \boldsymbol{C}^* \approx \delta \boldsymbol{C}_T^*$, where

$$\langle \boldsymbol{T}_1 \rangle (\delta \boldsymbol{C}_T^*)^{-1} = \boldsymbol{I} - \langle \boldsymbol{T}_2 \rangle \langle \boldsymbol{T}_1 \rangle^{-1} + \langle \boldsymbol{T}_1 \rangle \bar{\boldsymbol{G}}. \tag{63}$$

The condition (62) is satisfied if the structural correlations among the inclusions are small, even if their stiffness fluctuations are large. After some tensor algebra, we find from eq. (63) a novel expression for the effective material parameters:

$$\delta \boldsymbol{C}_T^* = \langle \boldsymbol{T}_1 \rangle \left(\boldsymbol{I} - \langle \boldsymbol{T}_1 \rangle^{-1} \mathbf{X} \right)^{-1}, \tag{64}$$

where

$$\mathbf{X} = \langle \boldsymbol{T}_2 \rangle - \langle \boldsymbol{T}_1 \rangle \bar{\boldsymbol{G}} \langle \boldsymbol{T}_1 \rangle. \tag{65}$$

Recall that $\langle \boldsymbol{T}_1 \rangle$ is given by eq. (52). It remains to evaluate $\mathbf{X}$.

From eqs (18), (52)–(54), (56) and (65), we obtain

$$\mathbf{X} = \sum_r \sum_s \boldsymbol{t}^{(r)} \langle \mathbf{A}^{(rs)} \rangle \boldsymbol{t}^{(s)} - \sum_r \boldsymbol{t}^{(r)} v^{(r)} \boldsymbol{G}^{(r)} \boldsymbol{t}^{(r)}, \tag{66}$$

where

$$\langle \mathbf{A}^{(rs)} \rangle = \int_\Omega d\mathbf{x}' \boldsymbol{G}^{(0)}(\mathbf{x} - \mathbf{x}') \left[\langle \bar{\theta}^{(r)}(\mathbf{x}) \bar{\theta}^{(s)}(\mathbf{x}') \rangle - \langle \bar{\theta}^{(r)}(\mathbf{x}) \rangle \langle \bar{\theta}^{(s)}(\mathbf{x}') \rangle \right], \tag{67}$$

depends only on $\boldsymbol{C}^{(0)}$ and the stochastic geometry of the microstructure. In Appendix B we use the method of Ponte Castaneda & Willis (1995) to evaluate the $\langle \mathbf{A}^{(rs)} \rangle$ parameters for a class of microstructures with prescribed two-point correlation functions having ellipsoidal symmetry for the distribution of the centres of arbitrarily shaped inclusions. The evaluation shows that

$$\langle \mathbf{A}^{(rs)} \rangle = \delta_{rs} v^{(r)} \boldsymbol{G}^{(s)} - v^{(r)} v^{(s)} \boldsymbol{G}_d^{(rs)}, \tag{68}$$

where

$$\boldsymbol{G}_d^{(rs)} = \int_{\Omega_d^{(rs)}} d\mathbf{x}' \boldsymbol{G}^{(0)}(\mathbf{x} - \mathbf{x}'), \quad \mathbf{x} \in \Omega_d^{(rs)}, \tag{69}$$

is a spatially invariant tensor since $\Omega_d^{(rs)}$ represents an ellipsoid having the same symmetry as $p^{(s|r)}(\mathbf{z} - \mathbf{z}')$ which, in turn, represents the probability density for finding an inclusion of type s centred at point $\mathbf{z}'$ given that there is an inclusion of type r centred at point $\mathbf{z}$. Since $p^{(s|r)}(\mathbf{z} - \mathbf{z}') = p^{(r|s)}(\mathbf{z}' - \mathbf{z})$ it follows that $\boldsymbol{G}_d^{(rs)} = \boldsymbol{G}_d^{(sr)}$. We have assumed that the inclusions do not overlap because an ellipsoid of type r is surrounded by a 'security' ellipsoid $\Omega_d^{(rs)}$, in the sense that $p^{(s|r)}(\mathbf{z}'') = 0$ if $\mathbf{z}'' \in \Omega_d^{(rs)}$. (Since $\Omega_d^{(rs)}$ must be chosen just large enough to exclude inclusion overlap, it is clear that our calculation will in some cases (for example in the case of spherical inclusions distributed with ellipsoidal symmetry) exclude those cases of very close inclusions which, although rare, will contribute a disproportionate amount to the 'interaction' terms. However, this appears to be a minor drawback which our method shares with that of Ponte Castaneda & Willis (1995). In the case of a composite consisting of inclusions characterized by the same ellipsoidal shape, however, the inclusions may come as close together as they want, if the aspect ratio of the correlation function is taken to be identical to that of the inclusions.) From eqs (66) and (68) we find that

$$\mathbf{X} = - \sum_r \sum_s \boldsymbol{t}^{(r)} v^{(r)} \boldsymbol{G}_d^{(rs)} \boldsymbol{t}^{(s)} v^{(s)}, \tag{70}$$

which means that we are now in a position to present an explicit expression for the effective elastic constants of a material with complex microstructure.

From eqs (52), (59), (64) and (70), we obtain a new expression;

$$\boldsymbol{C}_T^* = \boldsymbol{C}^{(0)} + \sum_r \boldsymbol{t}^{(r)} v^{(r)} \left\{ \boldsymbol{I} + \left[\sum_s \boldsymbol{t}^{(s)} v^{(s)} \right]^{-1} \sum_u \sum_v \boldsymbol{t}^{(u)} v^{(u)} \boldsymbol{G}_d^{(uv)} \boldsymbol{t}^{(v)} v^{(v)} \right\}^{-1}, \tag{71}$$

which becomes completely explicit and easy to use when the inclusions are ellipsoidal in shape. It is useful to note that the effect of spatial distributions is of higher order in the volume concentrations than the effect of the shape of the inclusions (Ponte Castaneda & Willis 1995). To see this, note that eq. (71) implies that

$$\boldsymbol{C}_T^* = \boldsymbol{C}^{(0)} + \sum_r \boldsymbol{t}^{(r)} v^{(r)} - \sum_r \sum_s \boldsymbol{t}^{(r)} v^{(r)} \boldsymbol{G}_d^{(rs)} \boldsymbol{t}^{(s)} v^{(s)} + O\left[(v^{(r)})^3 \right], \tag{72}$$

which agrees with Eshelby's (1957) dilute estimates to first order in the volume concentrations.

Since our goal is not only to obtain new estimates for the overall properties of a wide range of shale-related media, but also to place some of the most well-established approximations in this field on a common footing (so that we can investigate their limitations and connections), it will now be assumed that the spatial distribution is the same for all pairs of interaction inclusions, in the sense that $\boldsymbol{G}_d^{(rs)} = \boldsymbol{G}_d$ for all r and s. Aside for mathematical convenience, we see no rationale for this rather restrictive assumption, under which eqs (71) and (72) reduces to

$$\boldsymbol{C}_T^* = \boldsymbol{C}^{(0)} + \left[\sum_r \boldsymbol{t}^{(r)} v^{(r)} \right] \left\{ \boldsymbol{I} + \boldsymbol{G}_d \left[\sum_s \boldsymbol{t}^{(s)} v^{(s)} \right] \right\}^{-1}, \tag{73}$$

and

$$\boldsymbol{C}_T^* = \boldsymbol{C}^{(0)} + \sum_r \boldsymbol{t}^{(r)} v^{(r)} - \left(\sum_r \boldsymbol{t}^{(r)} v^{(r)} \right) \boldsymbol{G}_d \left(\sum_s \boldsymbol{t}^{(s)} v^{(s)} \right) + O\left[(v^{(r)})^3 \right], \tag{74}$$

respectively. Recall that $C^{(0)}$ can be selected rather arbitrarily. If we for a moment assume that $C^{(0)}$ is the tensor of elastic constants for a matrix phase that contains all the other phases as inclusions, then the estimate (73) reduces to that developed recently by Ponte Castaneda & Willis (1995), and the estimate (74) reduces to something new which in fact includes all the theories (or crack models) of Hudson (1980, 1981, 1988, 1994a,b) as special cases (see Appendix C; Douma 1988).

One should be very careful in using results that are second order in the inclusion concentrations, such as those in eqs (72) and (74), because they are 'doomed' to show unphysical increases of effective stiffnesses with increasing crack densities, at relatively low crack densities (see Cheng 1993). However, this does not mean that these (Hudson-consistent) second-order results are completely useless (as suggested by one of the reviewers). From the analysis of Kachanov (1993), it is clear that there exist an interval of crack density (or inclusion concentration) where the (Hudson-consistent) second-order approximations (are well behaved) can definitely be regarded as improvements on the corresponding first-order approximations. The problem is that this interval is often rather narrow (Kachanov 1993). (Hudson's second-order model typically breaks down when the crack density becomes larger than 0.1 or so (see Cheng 1993), whilst sedimentary rocks of interest to the petroleum industry may have crack densities as high as 0.3 or even higher (see Thomsen 1985).)

As pointed out by one of the reviewers, there exist many inherently 'approximate' methods, such as the so-called Mori–Tanaka estimate (which can be obtained from eq. (73), if we (consider one family of inclusions) set the aspect ratio of the correlation function equal to that of the inclusions (see Ponte Castaneda & Willis 1995)) or the differential effective medium (DEM) scheme [that can be derived from eq. (74) if we drop the second-order correction and do the analysis incrementally; inclusion concentration is increased in small steps, and $C^{(0)}$ is taken to be the effective stiffness tensor at each step (see Nishizawa 1982; Kachanov 1993; Hornby *et al.*1994a)], that normally gives physically plausible results, even when the crack densities (or inclusion concentrations) are no longer small. With the introduction of the *T*-matrix approach to shale acoustics, however, these inherently 'approximate' methods may no longer (be needed) represent the best solution to the problem of elastic inclusions at non-dilute concentrations. In addition, it is interesting to note that the (explicit) *T*-matrix approximation in eq. (71)/(73) is much easier to implement than the (implicit) DEM scheme. In fact, it is not more difficult to implement this *T*-matrix approximation than the inherently 'approximate' Mori–Tanaka estimate.

Ponte Castaneda & Willis (1995) concluded that their Hashin–Strikman-type approximation (represented by eq. 73) is in disagreement with the corresponding estimates of the Mori–Tanaka and differential types, and emphasized that these inherently 'approximate' methods do not explicitly account for the spatial distribution of inclusions. From the works of Nan *et al.* (1998) and Torquato (1998), it is clear that the effects of spatial distribution normally become increasingly important when the inclusion concentration increases beyond the dilute limit. The justification for using the inherently 'approximate' methods is partially intuitive, partially because of the physically reasonableness of the resulting behaviour, partially because of an improved agreement with experiment and not least because of their simplicity (Ponte Castaneda & Willis 1995). For all of these reasons, we prefer to take a higher-order *T*-matrix approach when estimating the overall properties of (cracked) shales from the parameters of the microstructure. However, we must admit that even the most general *T*-matrix approximation in eq. (71) may be invalid at high concentrations of inclusions. It appears to be difficult to determine the exact range of validity for the various *T*-matrix approximations, and so the best thing we can do (right now) is to proceed with a more qualitative discussion.

The variational analysis performed by Ponte Castaneda & Willis (1995) suggests that the preferred approximation in eq. (71)/(73) (having the same form as the exact formal solution in eq. 21) would work particularly well for an optimal matrix-inclusion system for which all correlation functions of order three or higher are identical to zero, as long as the 'security' ellipsoids surrounding the inclusions are not overlapping and the condition (62) is satisfied. Ponte Castaneda & Willis (1995) wrote that their approximation (represented by eq. 73) becomes identical to the Hashin–Strikman upper or lower bound, depending on what phase is singled out to serve as the matrix. Ponte Castaneda & Willis (1995) indicated that one can sometimes find the highest possible inclusion concentration where a particular approximation is strictly valid, if one knows the shapes of the inclusions and their spatial distributions. For the special case of a matrix material (phase 1) containing just one type of inclusions (phase 2), Ponte Castaneda & Willis (1995) found that their approximation is consistent with the impenetrability hypothesis only for certain combinations α_d, $\alpha^{(2)}$ and $v^{(2)}$, where α_d is the aspect ratio of the correlation function, $\alpha^{(2)}$ is the aspect ratio of the inclusions and $v^{(2)}$ is the volume concentration of the inclusions. Among other things they found that, when $\alpha_d > \alpha$, the minimum possible value of α for given α_d and $v^{(2)}$ is $\alpha|_{\min} = \alpha_d v^{(2)}$.

Further insight into the difficult problem of elastic inclusions at non-dilute concentration may be obtained if we realize that eqs (71)/(73) and (72)/(74) may be regarded as generalizations of eqs (51) and (47) in the paper of Zeller & Dederichs (1973), respectively. Zeller and Dederich write that 'the approximation (51) (special case of 71/73) would be exact for a fictive polycrystal consisting of a single anisotropic grain embedded in an isotropic matrix. In scattering theory the effective constants correspond to the optical potential. Thus, whereas the approximation (47) (special case of 72/74) represents the sum of the single scattering matrices, the improved approximation (51) (special case of 71/73) represents the sum of the single optical potentials or the sum of the single effective constants, respectively.' This gives us limited encouragement to proceed with the application of the (non-self-consistent) generalized 'optical potential approximation' or OPA (71)/(73) in situations involving finite concentrations of inclusions.

More encouragement is provided by Molinari & Mouden (1996), who claim that an expression for the overall properties of a composite that clearly is less general that given in eqs (71)/(73) is valid at non-dilute concentrations of inclusions, because it account for the interaction between the inclusions by using a cluster scheme somewhat different from that developed in the present study. This claim, in fact, forms the whole basis for the paper of Molinari & Mouden (1996) which, curiously enough, is also based on the pioneering work of Zeller & Dederichs (1973), but is much less general than the present one, partially because it is restricted to spherical inclusions.

To obtain reliable results on the basis of the T-matrix approach, it necessary (but not sufficient) to prevent the 'security' ellipsoids surrounding the inclusions from overlapping; we also need to consider the role of symmetry of the various components and to select an adequate reference medium (represented by $C^{(0)}$). Intuitively, it makes sense that the reference medium should be chosen to be similar to the effective environment experienced by the individual inclusions, so that we can minimize the effects of ignoring certain higher-order interaction terms (Zeller & Dederichs 1973). For the class of particulate microstructures consisting of a random distribution of inclusions of $F-1$ different types in a matrix of a homogeneous phase, a good choice for the reference material is the matrix material itself; particularly if the volume concentrations of inclusions are in the range from small to moderate (see Ponte Castaneda & Willis 1995).

In the case of a multiphase aggregate without a clearly defined matrix material and where each phase appears in the form of inclusions embedded in a sea of other inclusions, one of the things one can try to do is to set $C^{(0)} = C_T^*$ so that eqs (71) and (72) reduce to

$$\sum_r t_*^{(r)} v^{(r)} \left\{ I + \left[\sum_s t_*^{(s)} v^{(s)} \right]^{-1} \sum_u \sum_v t_*^{(u)} v^{(u)} G_{d*}^{(uv)} t_*^{(v)} v^{(v)} \right\}^{-1} = 0, \tag{75}$$

and

$$\sum_r t_*^{(r)} v^{(r)} - \sum_r \sum_s t_*^{(r)} v^{(r)} G_{d*}^{(rs)} t_*^{(s)} v^{(s)} \approx 0, \tag{76}$$

respectively. In the above equations we have added a '*'-symbol to $t^{(r)}$ and $G_d^{(rs)}$ to remind us that these tensorial quantities should now be evaluated for a homogeneous reference medium having the same elastic properties as the (yet to be determined) effective medium. The generalized self-consistent conditions (75) and (76) represent implicit equations for $C^{(0)} = C_T^*$. In the following we shall refer to them as generalized coherent potential approximations or CPAs, to keep the terminology consistent with that of quantum scattering theory. The possibility of developing such generalized CPAs has been discussed many times (e.g. Kroner 1986; Ponte Castaneda & Willis 1995), but this is the first time we have seen explicit expressions suitable for computer evaluation. If and only if $G_{d*}^{(rs)} = G_{d*}$ for all r and s then the generalized CPA reduces to the first-order CPA (Zeller & Dederichs 1973; Gubernatis & Krumhansl 1975):

$$\sum_r t_*^{(r)} v^{(r)} \approx 0, \tag{77}$$

which is equivalent to the usual symmetric self-consistent approximation (see Hershey 1954; Kroner 1958; Willis 1977; Berryman 1980a,b; Hornby *et al.* 1994);

$$C_T^* \approx \left[\sum_{r=1} v^{(r)} C^{(r)} \mathbf{Q}^{(r)} \right] \left[\sum_{s=1} v^{(s)} \mathbf{Q}^{(s)} \right]^{-1}, \tag{78}$$

where

$$\mathbf{Q}^{(r)} = \left[I + G_*^{(r)} \left(C^{(r)} - C_T^* \right) \right]^{-1}. \tag{79}$$

It may be noted that the unsymmetric class of 'self-consistent' theories studied by Hill (1965), Budiansky (1965) and others (see Berryman 1980b) does not yield the same results as the first-order CPA in eq. (77) (except for spherical inclusions), because one of the phases has been singled out to serve as the matrix. Berryman (1980b) showed how the derivation of this latter class of theories can be symmetrized to yield results that are consistent with the T-matrix approach.

When dealing with a composite which is not characterized by a well-defined matrix material, it clearly makes sense to use a symmetric self-consistent (coherent potential) approximation, but one could also try to use a symmetric non-self-consistent (optical potential) approximation, if one have any idea about what to use for $C^{(0)}$. (Inherently 'approximate' methods (like those discussed earlier) and/or physical intuition may be helpful when it comes to the selection of a suitable reference material.) It is interesting to note that, in the case of a two-phase composite consisting of solid and fluid inclusions that are treated symmetrically (for example, on the basis of the (Castaneda–Willis-consistent) OPA rather than the first-order CPA), at least one of the inclusion concentrations is necessarily large. Thus, the symmetric approximations may also become invalid, unless the comparison or reference material is chosen so that the stiffness fluctuations are sufficiently small. Therefore, it is becoming increasingly clear that, it is not only the volume concentrations that are important when discussing the range of validity of a given effective medium approximation. We are still not sure about the exact range of validity of the various approximations we have improved upon, but a kind of progress (or unification) have definitely been achieved.

7 SOME DETAILS FOR APPLICATION

Whereas the main analytical results of this paper has already been obtained by dividing the population of inclusions into families of inclusions having the same shape/stiffnesses and orientation, we now introduce a new population structure specially designed for media such as shales and certain cracked media having a partially aligned microstructure. Specifically, we re-divide the population of inclusions into new families of inclusions, the members of each new family having the same aspect ratio $\alpha^{(\rho)}$, orientation distribution function $O^{(\rho)}$, elastic stiffness tensor $C^{(\rho)}$ and rescaled volume concentration $v^{(\rho)}$, labelled by $\rho = 1, \ldots, \Phi$.

The orientation of an ellipsoidal inclusion with principal axes $OX_1X_2X_3$ with respect to a set of axes $Ox_1x_2x_3$ fixed in the reference material can be specified in terms of the three Euler angles θ, ψ and ϕ of Kroner (1986), which coincide with those of Morris (1969) and

Sayers (1994). (Different conventions exist for the three Euler angles.) If the orientation distribution of inclusions selected from the ρth set of inclusions is given by $O^{(\rho)}(\theta, \psi, \phi)$, θ is the angle between the OX_3 axis (coinciding with the short axis of the ellipsoidal inclusion under consideration) and the Ox_3 axis (coinciding with the main symmetry axis of the reference material, when $\boldsymbol{C}^{(0)}$ is a transversely isotropic tensor); ϕ represent a rotation of the $OX_1X_2X_3$ coordinate system around the OX_3 axis (see Kroner 1986).

If we denote by $\bar{\boldsymbol{t}}^{(\rho)}$ the orientation average of the *t*-matrix for a single inclusion selected from the ρth set, we may express the first-order correction in the form

$$\sum_{r=1}^{F} \boldsymbol{t}^{(r)} v^{(r)} \to \sum_{\rho=1}^{\Phi} \bar{\boldsymbol{t}}^{(\rho)} v^{(\rho)}, \tag{80}$$

which implies no loss of generality. However, the same statement for the second-order correction

$$\sum_{r=1}^{F} \sum_{s=1}^{F} \boldsymbol{t}^{(r)} v^{(r)} \boldsymbol{G}_d^{(rs)} \boldsymbol{t}^{(s)} v^{(s)} \to \sum_{\rho=1}^{\Phi} \sum_{\sigma=1}^{\Phi} \bar{\boldsymbol{t}}^{(\rho)} v^{(\rho)} \bar{\boldsymbol{G}}_d^{(\rho\sigma)} \bar{\boldsymbol{t}}^{(\sigma)} v^{(\sigma)}, \tag{81}$$

will only be true if the spatial distribution of inclusions is independent of the orientations, as we assume in the following. (Somewhat dangerously, here we are using the symbol σ as a summation index. In the above equation, σ has nothing to do with the stress field.) In eq. (81), we have introduced the tensor $\bar{\boldsymbol{G}}_d^{(\rho\sigma)}$, which is given by the usual expression for the $\boldsymbol{G}$ tensor of an ellipsoidal inclusion (eqs 37–39), provided that the aspect ratio of the associated inclusion is set equal to $\alpha_d^{(\rho\sigma)}$ which, in turn, determines the symmetry of the (translation-invariant) conditional probability density $\bar{p}^{(\sigma|\rho)}(\mathbf{x} - \mathbf{x}')$ for finding an inclusion with aspect ratio $\alpha^{(\sigma)}$ centred at point $\mathbf{x}'$ given that there is an inclusion with aspect ratio $\alpha^{(\rho)}$ centred at point $\mathbf{x}$, independent of the inclusion orientations.

The rearrangement of the inclusion population discussed above allow us to take into account possible correlations between inclusion shape and orientation. This is obviously useful when dealing with mixtures of partially aligned clay platelets and more rounded silt minerals. However, it may also be useful in a 'stressed' situation, where one can expect the aspect ratio to depend upon orientation, with cracks parallel to the direction of maximum principal stress having a larger mean aspect ratio then those perpendicular to it (see Gibson & Toksoz 1990). To ensure that the normalization stays correct, one must ensure that

$$\sum_{\rho=1}^{\Phi} v^{(\rho)} = \sum_{r=1}^{F} v^{(r)}, \tag{82}$$

so that the total porosity remains the same, and

$$\int_0^{\pi} d\theta \sin\theta \int_0^{2\pi} d\psi \int_0^{2\pi} d\phi O^{(\rho)}(\theta, \psi, \phi) = 1, \tag{83}$$

so that each inclusion is given an orientation.

The main task in this section is to evaluate $\bar{\boldsymbol{t}}^{(\rho)}$ by solving

$$\bar{\boldsymbol{t}}^{(\rho)} = \int_0^{\pi} d\theta \sin\theta \int_0^{2\pi} d\psi \int_0^{2\pi} d\phi O^{(\rho)}(\theta, \psi, \phi) \left\{ \boldsymbol{I} - \left[\boldsymbol{C}^{(\rho)}(\theta, \psi, \phi) - \boldsymbol{C}^{(0)} \right] \boldsymbol{G}\left(\theta, \psi, \phi; \alpha^{(\rho)}\right) \right\}^{-1} \left[\boldsymbol{C}^{(\rho)}(\theta, \psi, \phi) - \boldsymbol{C}^{(0)} \right] \tag{84}$$

(*cf*. eq. 25). The corresponding stiffness tensor is given by (the usual transformation law)

$$\boldsymbol{C}^{(\rho)}(\theta, \psi, \phi) = [\mathbf{a}(\theta, \psi, \phi) \otimes \mathbf{a}(\theta, \psi, \phi) \otimes \mathbf{a}(\theta, \psi, \phi) \otimes \mathbf{a}(\theta, \psi, \phi)] \boldsymbol{C}^{(\rho)}(0, 0, 0), \tag{85}$$

where the symbol $\otimes$ denotes the dyadic tensor (outer) product, and

$$\mathbf{a}(\theta, \psi, \phi) = \begin{pmatrix} \cos\phi & -\sin\phi & 0 \\ \sin\phi & \cos\phi & 0 \\ 0 & 0 & 1 \end{pmatrix} \begin{pmatrix} \cos\psi & -\sin\psi & 0 \\ \sin\psi & \cos\psi & 0 \\ 0 & 0 & 1 \end{pmatrix} \begin{pmatrix} \cos\theta & 0 & \sin\theta \\ 0 & 1 & 0 \\ -\sin\theta & 0 & \cos\theta \end{pmatrix}, \tag{86}$$

is a second-rank transformation tensor function of the three Euler angles (see Jeffreys & Jeffreys 1972), representing the non-Abelian symmetry group SO(3) (e.g. Weyl 1957; Nowick 1995).

As discussed by Mura (1982), there is a simple relationship between $\boldsymbol{G}(\theta, \psi, \phi; \alpha^{(\rho)})$ and $\boldsymbol{G}(0, 0, 0; \alpha^{(\rho)})$. Nevertheless, it is interesting to note that

$$\boldsymbol{G}(\theta, \psi, \phi; 1) = \boldsymbol{G}(0, 0, 0; 1) \tag{87}$$

(*cf*. eqs 37–39). Thus, the $\boldsymbol{G}$ tensor for a single spherical inclusion is independent of its orientation. This is an agreeable feature, because a spherical inclusion may, in fact, be used to represent the basic building block of shale structures, as discussed in the next section.

If and only if $\boldsymbol{C}^{(0)}$ is an isotropic tensor (that is, virtually never when dealing with shales), the *t*-matrix for a single inclusion selected from the ρth set satisfies a relationship similar to that for the corresponding stiffness tensor in eq. (85), and we can use the analytical averaging method of Sayers (1994) to evaluate $\bar{\boldsymbol{t}}^{(\rho)}$. Generally, the orientation averaging needs to be done numerically. Nevertheless, it is possible to establish a kind of link between the *T*-matrix approach and the simple shale model of Sayers (1994). To see this, we now write the orientation distribution function $O^{(\rho)}$ as a series of generalized Legendre functions Z_{lmn} of $\cos\theta$; that is,

$$O^{(\rho)}(\theta, \psi, \phi) = \sum_{l=0}^{\infty} \sum_{m=-l}^{l} \sum_{n=-l}^{l} W_{lmn}^{(\rho)} Z_{lmn}(\cos\theta) e^{-im\psi} e^{-in\phi}. \tag{88}$$

Using the orthogonality relations between these functions (Sayers 1994), we obtain

$$W_{lmn}^{(\rho)} = \frac{1}{4\pi^2} \int_0^\pi d\theta \sin\theta \int_0^{2\pi} d\psi \int_0^{2\pi} d\phi\, O^{(\rho)}(\theta, \psi, \phi) Z_{lmn}(\cos\theta) e^{im\psi} e^{in\phi}. \tag{89}$$

Since the t-matrix is actually a tensor of fourth rank, its orientation average depends only on the coefficients $W_{lmn}^{(\rho)}$ of the expansion of $O^{(\rho)}(\theta, \psi, \phi)$ for $l \leq 4$. If the orientation distribution is symmetric about the axis $\theta = 0$ (as we assume in the following) then the parameters $W_{lmn}^{(\rho)}$ are zero unless $m = n = 0$, and so we can replace $O^{(\rho)}(\theta, \psi, \phi)$ by a simplified function $O^{(\rho)}(\xi)$ of $\xi = \cos\theta$ only. In addition, we note that $O^{(\rho)}(\xi) = O^{(\rho)}(-\xi)$ and so $W_{l00}^{(\rho)}$ is zero unless l is even (Sayers 1994). It is clear from the paper of Roe (1965) that

$$Z_{l00}(\xi) = \sqrt{\frac{2l+1}{2}} P_l(\xi), \tag{90}$$

where P_l is a Legendre polynomial of order l; $P_0(\xi) = 1$, $P_2(\xi) = \frac{1}{2}(3\xi^2 - 1)$ and $P_4(\xi) = \frac{1}{8}(35\xi^4 - 30\xi^2 + 3)$. Using eqs (83), (89) and (90), we find that the non-zero $W_{lmn}^{(\rho)}$ coefficients are (under the above circumstances) given by

$$W_{000}^{(\rho)} = \sqrt{\frac{1}{2}} \frac{1}{4\pi^2}, \tag{91}$$

$$W_{200}^{(\rho)} = \sqrt{\frac{5}{2}} \int_{-1}^1 d\xi\, O^{(\rho)}(\xi) P_2(\xi), \tag{92}$$

$$W_{400}^{(\rho)} = \sqrt{\frac{9}{2}} \int_{-1}^1 d\xi\, O^{(\rho)}(\xi) P_4(\xi). \tag{93}$$

Given measurements of the effective stiffnesses of a textured composite and measurements of the $W_{lmn}^{(\rho)}$ as can obtained from the inversion of pole figures associated with X-ray diffraction experiments (Roe 1965) or the examination of scanning electron microphotographs (Hornby *et al.* 1994; Sayers 1994), the effective stiffnesses at arbitrary orientation distributions may be predicted by changing the values of the $W_{lmn}^{(\rho)}$. The use of a limited number of $W_{lmn}^{(\rho)}$ corresponds to the specification of the orientation distribution by its first few moments, which may aid us in the interpretation of acoustic measurements on anelliptical shales (Sayers 1994).

Although the simplified (cylindrically symmetric) orientation distribution functions are functions of one variable only, eqs (84), (88) and (90) suggest that we still need to solve a suite of 3-D integrals to evaluate the $\bar{t}^{(\rho)}$ matrices; that is,

$$\bar{t}^{(\rho)} = \int_{-1}^1 d\xi \int_0^{2\pi} d\psi \int_0^{2\pi} d\phi \left[\frac{1}{8\pi^2} + \sqrt{\frac{5}{2}} P_2(\xi) W_{200} + \sqrt{\frac{9}{2}} P_4(\xi) W_{400} \right]$$
$$\times \left\{ I - \left[C^{(\rho)}(\xi, \psi, \phi) - C^{(0)} \right] G\left(\cos^{-1}\xi, \psi, \phi; \alpha^{(\rho)} \right) \right\}^{-1} \left[C^{(\rho)}(\xi, \psi, \phi) - C^{(0)} \right], \tag{94}$$

where we have changed the integration variable from θ to $\xi = \cos\theta$. There exists an extensive body of literature discussing efficient approximation techniques for such integrals (Gubernatis & Krumhansl 1975), but the computing time may sometimes be longer than we want. Therefore, the list of possible simplifications should not stop here.

When dealing with shales, it often makes sense to assume $C^{(\rho)}$ to be (transversely isotropic) invariant with respect to rotations of the $OX_1X_2X_3$ system around the OX_3 axis, and the inclusions to be spheroidal in shape; so that we are free to set $\phi = 0$ in the above equations (due to the physical interpretation of the Euler angle ϕ, discussed earlier). Under the assumption that the system is cylindrically symmetric in the widest sense, we find from eq. (94) a 2-D integral;

$$\bar{t}^{(\rho)} = 2\pi \int_{-1}^1 d\xi \int_0^{2\pi} d\psi \left[\frac{1}{8\pi^2} + \sqrt{\frac{5}{2}} P_2(\xi) W_{200} + \sqrt{\frac{9}{2}} P_4(\xi) W_{400} \right]$$
$$\times \left\{ I - \left[C^{(\rho)}(\xi, \psi, 0) - C^{(0)} \right] G\left(\cos^{-1}\xi, \psi, 0; \alpha^{(\rho)} \right) \right\}^{-1} \left[C^{(\rho)}(\xi, \psi, 0) - C^{(0)} \right], \tag{95}$$

which can be solved sufficiently fast, for example using Gaussian quadrature.

Having shown how to evaluate the first- and second-order corrections, it should be relatively easy to implement the various T-matrix approximations we have derived in this paper on a computer, for example using the popular Matlab system. As shown earlier, the T-matrix estimation schemes are either explicit (non-self-consistent) or implicit (self-consistent). The implicit ones generally require the use of iterative techniques for their implementation (see Gubernatis & Krumhansl 1975; Diz & Humbert 1992; Jakobsen *et al.* 2000). Whatever estimation scheme one chooses to implement, it may be tempting to introduce the matrix representation of fourth-rank tensors (having the same symmetries as the elastic stiffness tensors) associated with the well-known notation of Voigt. This is particularly true since Auld (1990) has given an efficient recipe for doing tensor transformations in abbreviated subscripts (the Bond transformation, associated with eq. 85). However, it may be noted that the notation of Kelvin (1856) is more efficient for the computations since operations with the 6×6 matrices can be performed according to the usual matrix rules (see Weyl 1957; Nowick 1995). The Kelvin notation represents an isomorphism between the tensor and matrix components that can be explained as follows. First, for a given tensor $\{A_{ijkl}\}$, pairs of indices ij and kl are converted to single indices α and β by the standard convention $11 \to 1$, $22 \to 2$, $33 \to 3$, $23, 32, \to 4$, $13, 31, \to 5$, $12, 21, \to 6$. Next, each tensor element A_{ijkl} is associated with a matrix element $A_{\alpha\beta}$ by the rules

$$A_{ijkl} = A_{\alpha\beta}, \quad \alpha, \beta \leq 3,$$

$A_{ijkl} = \sqrt{2}A_{\alpha\beta}, \quad \alpha \text{ or } \beta > 3,$

$A_{ijkl} = 2A_{\alpha\beta}, \quad \alpha, \beta > 3.$

The resulting (Kelvin) matrices are of rank 6.

8 SHALE ACOUSTICS FROM A MODERN PERSPECTIVE

We now proceed with a more practical section, presenting a new method for estimating the effective stiffnesses of cracked shales from the parameters of the microstructure. To establish contact with the microworld, let us look at a scanning electron microphotograph (SEM) of a typical shale sample: in Figure 1 in the paper by Hornby *et al.* (1994), the plate-like and the more rounded particles are the clay and silt minerals, respectively. It appears that the clay platelets are fully aligned locally, but vary in orientation on a larger scale. The silt minerals (most notably quartz) seem to control the local misalignment of the clay platelets and the fluid-filled gaps between them. The system is very complicated, and so progress in theoretical shale acoustics may depend on our ability to identify their most essential morphological features. According to Hornby *et al.* (1994), it is important to focus on the problem of symmetry of the various components, and in particular on the role of connectivity.

In what follows, we shall first try to improve on the three-step modelling procedure for uncracked shales introduced by Hornby *et al.* (1994), and then introduce an additional step dealing with the effects of cracks (in a way which is more general than that of Hudson 1994b). For simplicity, we shall use nothing but an isotropic correlation function in connection with steps 1 and 2. The effect of using different spatial distributions for the positions of the inclusions making up a real shale model without and with cracks will, however, be illustrated in connection with steps 3 and 4, respectively.

8.1 A perfect shale

Following Hornby *et al.* (1994), we begin by estimating the effective elastic properties of the basic building block of shale structures; that is, a perfect shale composed of clay and fluid inclusions that are fully aligned. For a transversely isotropic medium (e.g. a perfect shale), the non-zero components of the elastic stiffness tensor are (in the notation of Voigt) $c_{11} = c_{22}, c_{33}, c_{44} = c_{55}, c_{66}, c_{13} = c_{23}$ and $c_{12} = (c_{11} - 2c_{66})$ (e.g. Musgrave 1970). If the total porosity and clay content of the real shale is denoted by ϕ and v_c, respectively, then the appropriate porosity for the corresponding perfect shale is obviously given by $\phi/(\phi + v_c)$. The problem in this subsection is to estimate the effective elastic stiffnesses of a perfect shale as a function of its fluid-filled porosity.

The shapes of the inclusions making up the shales need to be estimated before we can start the modelling. SEM pictures (e.g. fig. 1 in the paper by Hornby *et al.* 1994; Bennett *et al.* 1991) show that the clay platelets are approximately ellipsoidal in shape. According to Hornby *et al.* (1994), the shape of the clay platelets may actually be represented by an oblate spheroidal inclusion having an aspect ratio of 1/20. The fluid-filled gaps between the clay platelets are of angular shape, but will generally be elongated to the same degree as the platelets, and so Hornby *et al.* (1994) approximated these with the same oblate spheroidal shape as for the clay platelets. One might try to represent the shapes of these fluid-filled gaps by a whole spectrum of relatively low-aspect-ratio oblate spheroidal pores; each aspect ratio is given by a rather complicated function of several variables, including the applied stress (see Sayers 1999), the pore fluid pressure (see Hornby 1994), the porosity, the degree of compaction, the diagenetic state and the depth of burial. Realizing that there are great practical problems associated with this approach, we tend to follow Hornby *et al.* (1994) and Sams & Andrea (2001) in replacing the full spectrum of pore aspect ratios by a single effective aspect ratio; often found to be pretty close to the value of 1/20 suggested by Hornby *et al.* (1994).

The elastic constants of pure clay minerals are also needed as input parameters to the modelling. Unfortunately, these are not as well documented as are the values for silt minerals such as quartz and feldspar (Hornby *et al.* 1994). One reason for this unfortunate situation is that clay minerals do not exist as large minerals, and so it is difficult to measure their mechanical properties. Hornby *et al.* (1994) derived clay properties from experimental measurements on clay–fluid composites by inference from the self-consistent approximation, and under the simplifying assumption that the elastic properties of the clay–fluid composite as well as the pure clay minerals are isotropic. Wang *et al.* (2001) also derived clay properties from experimental measurements on clay-bearing composites, but still under the assumption that everything is isotropic. In reality, the elastic properties of the clay–fluid composite and the pure clay minerals may be anisotropic. Katahara (1996) found that pure/dry clay minerals behave as TI media characterized by five independent elastic constants. The problem is that the elastic stiffnesses recovered from measurements on pure/dry clay minerals by Katahara (1996) are unreasonably high compared with those inferred from velocity measurements on fluid-saturated and clay-bearing rocks by Hornby *et al.* (1994) and the rest of the mainstream of workers in this field (see Katahara 1996). Following Katahara (1996), we may only speculate why this is the case: the softening of the clay minerals due to the fluid, flat compliant cavities, chemical effects (see Sherwood 1993) and electrostatic forces (that tend to bind the fluid to the high surface area of the clay platelets). For simplicity, we shall stick to the isotropic clay properties of Hornby *et al.* (1994), which have already resulted in a reasonable match between theoretical predictions and ultrasonic measurements on a shale.

Our main interest lies in the performance of the individual approximations, and the various ways they may be combined to reflect the most essential morphological features of the objects we are modelling. According to Hornby *et al.* (1994), a perfect shale is identical to a biconnected clay–fluid composite; that is, a porous clay medium where the clay phase is load-bearing and the pore structure contains fluid
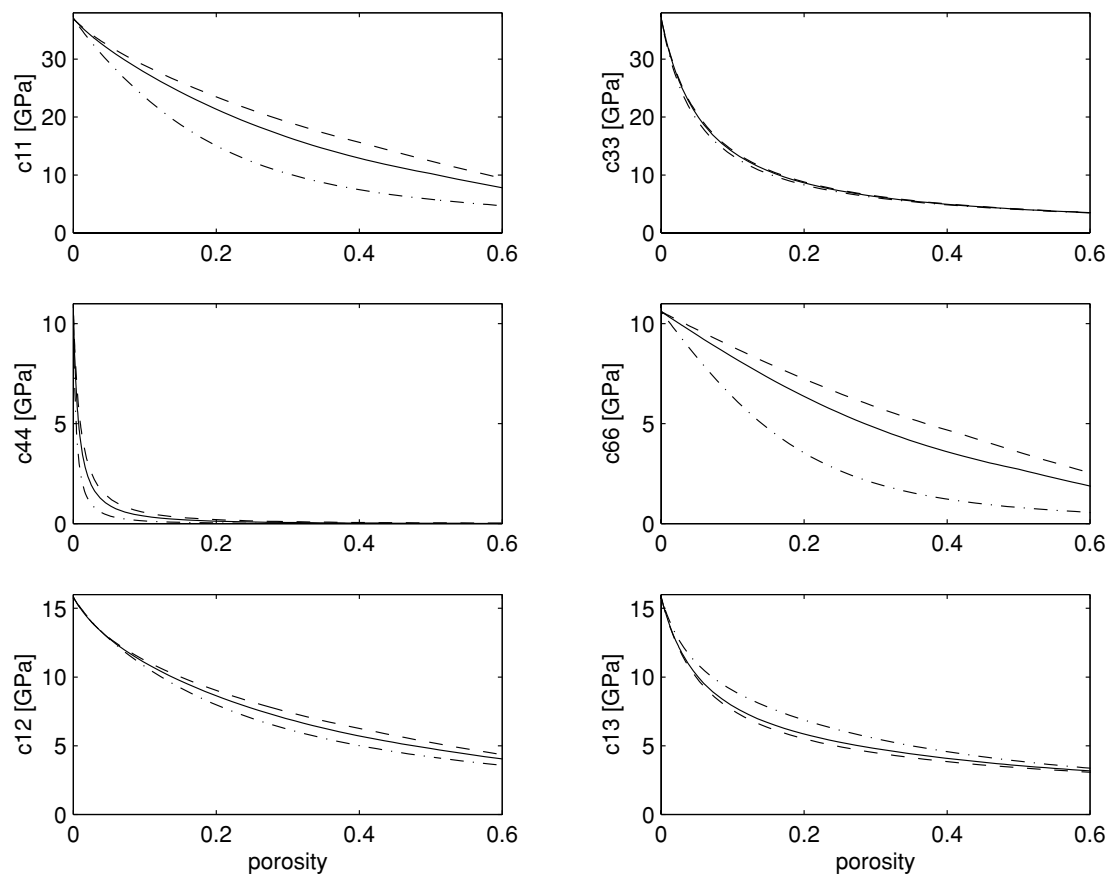
Figure 1. Computed effective stiffnesses for a fully aligned clay–water composite composed of oblate spheroidal inclusions having an aspect ratio of 1/20. We have tested the combined CPA/DEM approximation. The (solid, dashed, dashed-dotted) line type represents an initial CPA porosity of (42, 50, 58) per cent.

pathways implying non-zero permeability. If the issue of fluid connectivity really is important in shale acoustics then it is an unfortunate feature that biconnected composites such as perfect shales cannot be constructed simply using the CPA alone, since this approximation appears to yield a biconnected clay–fluid composite only over a narrow porosity range (between 40 and 60 per cent for inclusions that are spherical in shape; Berryman 1980a; Sheng 1990).

The procedure used by Hornby *et al.* (1994) to construct a clay–fluid composite that appears to be biconnected at all porosities can be described as follows. Beginning with an effective medium generated using the CPA at a fluid-filled porosity where that approximation apparently yields a biconnected material presumably still between 40 and 60 per cent, although the inclusions are no longer spherical in shape; Hornby 1994; Mainprice 1997), the overall properties are computed at the appropriate porosity for the perfect shale using the differential effective medium approximation, which is interpreted to preserve connectivity (see Sheng 1990; Hornby *et al.* 1994; Jakobsen *et al.* 2000).

Fig. 1 shows the effective elastic stiffnesses of a perfect shale estimated using the combined CPA/DEM theory. We have tested the effect of using different starting porosities for the CPA calculation. It appears that the results are very sensitive to this starting porosity, suggesting that the combined CPA/DEM theory is associated with significant uncertainties.

In our opinion, it is not clear if an effective medium model for perfect shales really needs to assign connectivity to the fluid phase. [After all, real shales are normally characterized by an extremely small permeability. During the passage of ultrasonic waves, considered by Hornby *et al.* (1994), it is more than possible that the fluid within the shale had little time and/or opportunity to move (see Hudson *et al.* 1996; Xu 1998; Jakobsen *et al.* 2003).] What is clear is that the microstructural interpretations of the CPA and DEM theories, that form the basis for the combined CPA/DEM theory of Hornby *et al.* (1994), are controversial (e.g. Mainprice 1997). Gueguen *et al.* (1997) claim that the percolation threshold (where the fluid phase becomes connected) predicted by the CPA corresponds with the use of a theory (in an extremely heterogeneous situation) outside its range of validity. This last statement may or may not be true (see Kachanov 1994), but one could perhaps avoid the whole issue by simply using the first-order CPA alone (and hopefully within its range of validity) when modelling the anisotropic elastic properties of a perfect shale.

One of the reviewers suggested (curiously enough) that the point concerning the connectivity of the fluid has nothing to do with permeability or squirt flow issues. In an attempt to clarify this point, consider a two-phase composite involving a solid phase that is connected (load-bearing) and a fluid phase that may or may not be connected (percolating). If the fluid phase is not connected then fluid pathways for global (Darcy) flow do not exist, but there may exist opportunities for local (squirt) flow (between neighbours belonging to the same cluster of pores). If the fluid phase is connected then there may obviously exist opportunities for global as well as local flow. Thus, it appears that the
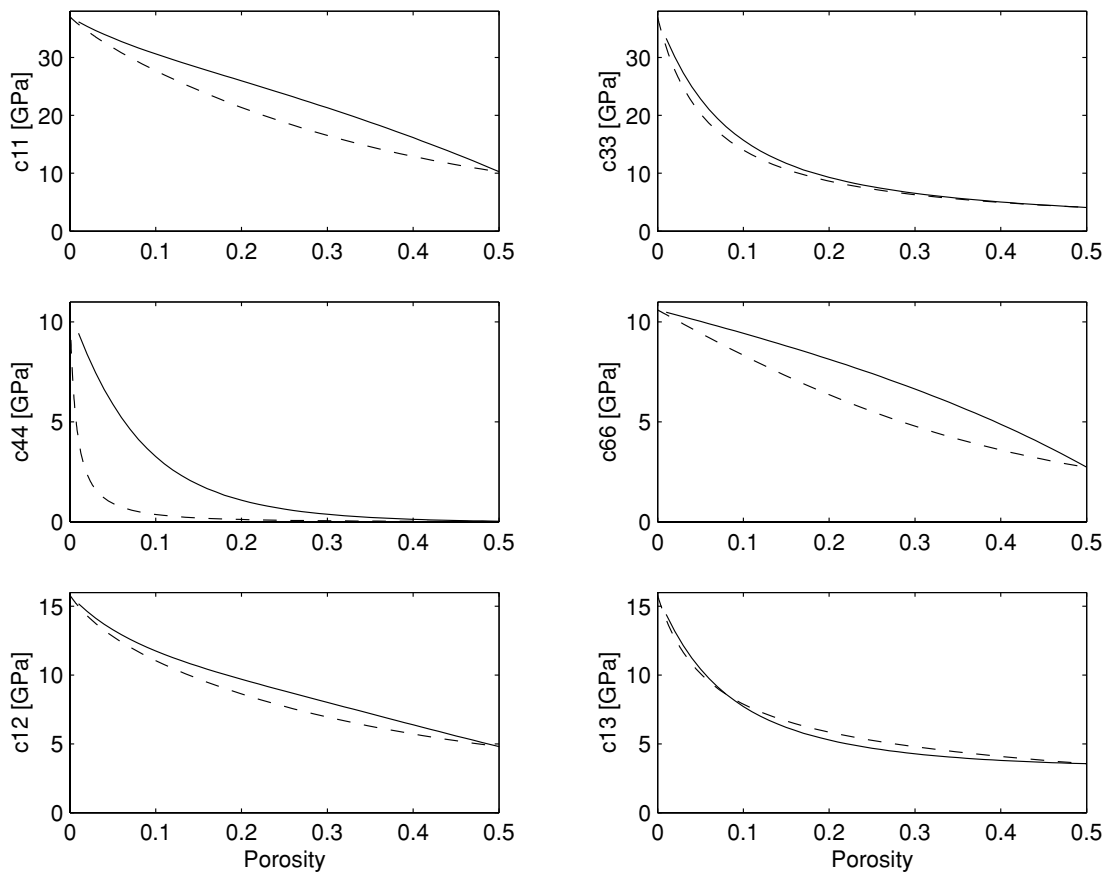
Figure 2. Virtually the same clay–fluid system as in Fig. 1, but now we are comparing the predictions of the combined CPA/DEM approximation (corresponding with an initial CPA porosity of 50 per cent) with those of the CPA alone (solid line).

point about the connectivity of the fluid is more related with the overall permeability than with the microscopic phenomenon of squirt flow (see also Berryman 1992). At the same time, we can see that the combined CPA/DEM model (which does not include the permeability tensor as a set of parameters) does not allow for squirt flow, because the fluid-filled pores within the associated clay–fluid composite have the same shape and orientation. (As detailed by Jakobsen *et al.* (2002), it is required that the shapes and/or orientations of the neighbouring pores be different, for local pressure gradients to exist and drive the squirt flow.)

In the opinion of Dr Xu (personal communication, 2000), the connectivity argument may indeed be applicable for the (qualitative) simulation of (fluid) transport properties (at the macroscopic level) but can be misleading when modelling effective elastic properties. Dr Xu speculated that the whole issue of effective medium theory is how to search for the elastic properties of the homogeneous reference medium (represented by the arbitrary stiffness tensor $C^{(0)}$). From the similarity of the T-matrix approximations with the Hashin–Strikman estimates of Ponte Castaneda & Willis (1995), we may follow Dr Xu in noting that, if the solid phase is selected as the matrix material (the fluid phase is unconnected), we have an upper bound; if the fluid phase is selected as the reference medium (the fluid phase is percolating) we have a lower bound. Any reference medium having physical properties between the two extremes could (in the opinion of Dr Xu) result in a bi-connected microstructure, to a certain degree. In other words, both the CPA and the DEM used by Hornby *et al.* (1994) could result in a bi-connected system (possibly to a different degree). In a practical sense, it could therefore be alright to combine the two schemes, in an attempt to make the model work. The problem is that there appears to exist a range of different combinations that are equally plausible but produce markedly different results.

It is difficult to tell if one approximation is better than another without having enough high-quality experimental data to compare with. What we are doing in this paper is basically to point out different theoretical possibilities that are more or less equally plausible. The basic philosophy behind this study was to investigate how far we can go in theoretical shale acoustics by only using effective medium approximations that can be derived using the rigorous T-matrix approach. For simplicity and many other reasons (see Mainprice 1997), it is tempting to try to model perfect shales without the rather controversial CPA/DEM theory, which may nevertheless represent a promising effective medium scheme for certain shale-related media (see Jakobsen *et al.* 2000).

Fig. 2 shows that the differences between the predictions of the CPA/DEM and the first-order CPA are not that large (compared with the large uncertainties associated with the CPA/DEM theory, the pore structures of shales and the elastic properties of pure clay), although the CPA at all fluid-filled porosities predicts significantly larger values for the out-of-plane shear modulus c_{44}.

If we assume finally that we can safely ignore the connectivity of the fluid phase, it would not be a good idea to model perfect shales on the basis of the DEM (alone), because the DEM (in contrast with the CPA) treats the clay and fluid inclusions in an unsymmetric manner (not compatible with Figure 1 in the paper by Hornby *et al.* 1994). It would probably not be a good idea to use an OPA either, because a symmetric treatment of the clay and fluid inclusions (within this framework) would require that we use something other than pure clay to represent the matrix material. (If we simply add fluid-filled flat pores into a homogeneous matrix of clay then we ignore effects related to the non-spherical nature of the clay platelets.) Since we do not have a natural reference material at this stage, the CPA appears to represent a relatively good alternative.

8.2 A less perfect shale

Following Hornby *et al.* (1994), we proceed by considering a less perfect shale consisting of an aggregate of crystals, each crystal being a unit of the perfect shale. The crystals are oriented according to a known statistical pattern, and it is required to find the overall properties of the aggregate. Progress along these lines requires the solution to two problems. The first is related with the fact that Hornby *et al.* (1994) developed a system for deriving the crystal orientation distribution function from a scanning electron microphotograph of a vertical slice of a shale sample. (SEM data are digitized and processed to obtain a 2-D array of image intensities for preferential orientations of the crystals. See also Bennett *et al.* (1991).) Secondly, we need to identify a sufficiently accurate effective medium approximation for polycrystals.

Historically, there has been a lot of work on the elasticity of polycrystals (see Hirsekorn 1990), but only the simplest approximations have received attention in theoretical shale acoustics. Voigt (1887) assumed the strain to be the same and hence equal to its mean value in each crystal, and found that the effective elastic stiffness tensor of the polycrystal is given by the ensemble average of the single-crystal stiffness tensors over all orientations. (This simple procedure forms the basis of the shale model of Sayers 1994.) Reuss (1929) assumed the stress to be the same and hence equal to its mean value in each crystal, and found that the effective elastic compliance tensor of the polycrystal is given by the ensemble average of the single crystal compliance tensors over all orientations. (The corresponding effective stiffness tensor is then found by inverting the effective compliance tensor.) Hill (1952) proved that the polycrystalline moduli calculated after Voigt and Reuss are upper and lower bounds for the true effective elastic moduli of the polycrystal and recommended using the mean values of both approximations.

It is clear that one should always employ an effective medium approximation for polycrystals that lies between the bounds of Voigt and Reuss. From a theoretical point of view, however, it seems somewhat unsatisfactory to simply take the arithmetic mean of the upper and lower bound (Hornby *et al.* 1994). Thomsen (1972) claimed that this so-called Hill average has no more theoretical justification than it has experimental support. However, a limited amount of experimental support for the phenomenological Hill average has actually been obtained, for example, by Bunge (1974) and Mainprice & Humbert (1994). The simple Hill average may therefore be good enough for many practical applications (e.g. Hirsekorn 1990; Mainprice & Humbert 1994), at least as a starting point for perturbative calculations (e.g. Sisodia & Verma 1990). If the Hill average is close to the actual solution (as suggested by Hornby *et al.* 1994) then it may be a good idea to let the arbitrary tensor $C^{(0)}$ represent the Hill average itself, and then calculate the corresponding correction terms using the (explicit) OPA, eq. (73). Alternatively, one may go one step further and solve the (possibly more accurate but implicit) first-order CPA, eq. (75), iteratively using the OPA as the first iteration.

Having studied a significant body of literature (e.g. Zeller & Dederichs 1973; Domany *et al.* 1975; Gubernatis & Krumhansl 1975; Christensen 1976; Kroner 1986; Middya & Basu 1986; Hirsekorn 1990; Humbert *et al.* 1991) we are left with the impression that the (original symmetric self-consistent approximation) first-order CPA is a very reasonable theory for the effective elastic constants of polycrystals. The single-phase aggregates we are dealing with here are indeed characterized by rather symmetric microstructures. (It is only when all crystal orientations are equally plausible that the microstructure of a polycrystal is completely (rotational) symmetric, but we always have an infinite number of 'phases', corresponding to a continuous distribution of (random) crystal orientations.) However, it may not be obvious what homogeneous reference medium the stiffness fluctuations (associated with the various crystal orientations) should be computed relative to, since the crystals are embedded in a sea of other crystals, without a well-defined matrix material. Since the constant tensor $C^{(0)}$ (characterizing the elastic properties of the homogeneous reference medium) is arbitrary, one may try to choose $C^{(0)}$ so that as many terms as possible vanish in the T-matrix expansion (Zeller & Dederichs 1973). By letting $C^{(0)}$ represent the elastic properties of the (yet to be determined) effective medium, we do not only follow our intuition, but also ensure that many higher-order interaction terms vanish (see Zeller & Dederichs 1973).

Zeller & Dederichs (1973) gave the impression that the first-order CPA includes more interaction terms than virtually all other simple approximations. Gubernatis & Krumhansl (1975) gave the same impression, and even proposed using the diagrammatic techniques of modern physics to make sense of it all. In this paper, we have proceeded with the application of 'modern' methods into the complex realm of shale acoustics, and arrived at a higher-order CPA that includes more interaction terms than ever before, because it explicitly takes into account the effects of possible correlations in the orientations and positions of two crystals only. As indicated in the discussion of eq. (81), however, it is not particularly easy to model such correlation effects within the framework of the higher-order CPA. Fortunately, the full complexity of the higher-order CPA may not be required when modelling perfect shales (without silt and cracks). Since the crystals in our model are assumed to be spherical in shape, we now see the reason for introducing correlation functions that are not spherically symmetric at this stage, and so we restrict ourselves here to conditions under which the higher-order CPA (in eq. 75) degenerates to the (usual self-consistent approximation) first-order CPA (in eq. 77).

Hirsekorn (1990) concluded that the first-order CPA is the most accurate and theoretically well-founded static method for computing effective elastic constants of polycrystals. In fact, this (first-order CPA) self-consistent method is generally accepted to give the best estimate (Mainprice & Humbert 1994). Unlike the Reuss, Hill and Voigt averages, the first-order CPA fulfils the boundary conditions for stress and strain statistically exactly (Kroner 1986; Hirsekorn 1990). However, the evaluation of first-order CPA is rather lengthy, and, in many cases, its predictions are often rather close to the simple Hill average (Hirsekorn 1990; Mainprice & Humbert 1994). For crystals (or grains) that are spherical in shape, the difference (between the predictions of the first-order CPA and the Hill average) was found by Morris (1970) to be less than 3 per cent. (In a comparison with experimental data discussed by Humbert *et al.* (1991), it was possible to see that the first-order CPA performed slightly better than the simple Hill average, although crystals were assumed to be spherical in shape.) For crystals that are not spherical in shape, Hendrix & Yu (1998) found that the difference between the predictions of the first-order CPA and the Hill average could be as high as 10–15 per cent, depending on what aspect ratio is used in the CPA to characterize the ellipsoidal shape of the single crystal. Sayers (1994) indicated that the (domains of preferential clay platelet alignment) crystals are indeed ellipsoidal in shape. However, it may be difficult to determine the aspect ratio of these crystals (or domains) for a wide range of shales, and so we shall not relax on the (simplifying) assumption that they are spherical in shape.

If one wants to use an approximation that is sensitive to the shape of the crystals (and takes into account the effects of possible correlations in the positions of differently oriented crystals), one could try to use an OPA (in conjunction with a suitable reference medium) in place of the (higher-order) CPA. The OPA appears to be particularly attractive when it comes to the inverse problem (see Johansen *et al.* 2002). Unlike the CPA (which requires the use of time-consuming iterative techniques for its implementation), the OPA represents a fast explicit scheme for estimating the effective stiffnesses of polycrystals. In this subsection, the OPA (with isotropic correlation functions), as well as the first-order CPA, have been tested for forward modelling only. To obtain the numerical results (discussed below), we combined the simplest CPA eq. (77), and the even simpler OPA eq. (73), with the numerical method for averaging over the crystal orientations associated with eqs (80) and (95).

Fig. 3 shows a comparison of different estimates for the effective elastic properties of a crystalline aggregate. The properties of the single crystal are identical to those in our model of a perfect shale, at three different water-filled porosities. It is apparent that the Voigt and Reuss averages are widely separated, but the OPA (with isotropic correlation functions) and (the first-order) CPA for spherical crystals seems to be very close to the Hill average. (In fact, the predictions of the CPA and the OPA are so close to the Hill average that one can hardly identify the various curves.)

8.3 A real shale

In the modelling procedure of Hornby *et al.* (1994), the DEM scheme is used to increase the concentration of a particular silt phase from zero to its final value, so that the concentration of the other phases changes in proportion to their relative concentrations in the aggregate (initially identical to the less perfect shale). Hornby *et al.* argued that by using the DEM scheme to add silt, they could ensure that these minerals did not become connected (even at relatively high volume concentrations), because the DEM scheme does not predict any percolation threshold (see Sheng 1990; Gueguen *et al.* 1997).

We all have sympathy with the care Hornby *et al.* took to ensure that the silt phases were disconnected. As pointed out by one of the reviewers, a connected silt phase would lead to a dramatically higher shear modulus for the shale, since silt has a higher shear modulus than clay (see Table 1). However, we are not sure that the DEM scheme represents the only alternative when it comes to the treatment of real shales as elastic composites (including silt). From a theoretical point of view, it is somewhat unsatisfactory that the DEM results are path dependent (see Berryman 1992; Kachanov 1994), which means that the results are (a little) sensitive to the order in which the various silt phases are added to the composite. More seriously, the DEM scheme treats the silt inclusions and the randomly oriented units of the perfect shale in an asymmetric manner (discussed by Berryman 1992), which may not be compatible with Figure 1 in the paper by Hornby *et al.* (1994).

We do not claim that it is completely wrong to use the DEM scheme at this stage; we are only trying to identify possible weak points and to come up with more or less equally plausible alternatives (that may produce markedly different results). After all, we are dealing with rather complex porous media, and it is often difficult to tell what is the most accurate effective medium approximation for a given microstructure. Even if it was correct that the DEM scheme represents the best way to add silt, it would be interesting to note that the (implicit and time-consuming)

Table 1. Relative volume concentrations and mechanical properties of the various mineral phases making up the solid fraction of the real shale under consideration. The bulk and shear moduli are given in units of GPa.

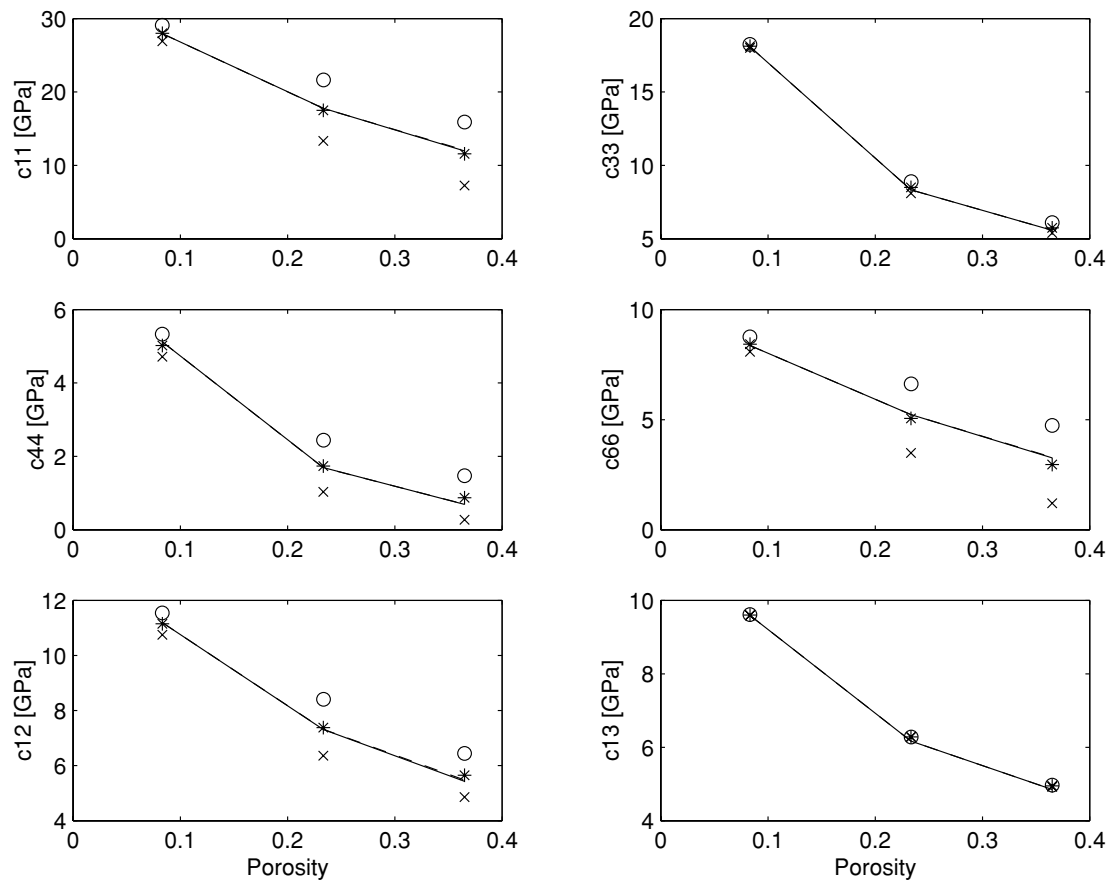| Mineral	Volume percentage	Bulk modulus	Shear modulus
Quartz	31	37.9	44.3
Plagioclase feldspar	2	75.6	25.6
K feldspar	2	75.6	25.6
Pyrite	5	147.4	132.5
Calcite	1	76.8	32.0
Dolomite	1	94.9	45.0
Clay	58	22.9	10.6

Figure 3. Comparison of different estimates for the effective elastic properties of a crystalline aggregate. The properties of the single crystal are identical to those of the fully aligned clay-water composite. We consider three different water volume concentrations. The Voigt, Reuss and Hill averages are denoted by 'o', 'x' and '*', respectively. The results of the CPA and OPA are represented by solid and dashed lines, respectively. We have used the Gaussian clay particle orientation distribution function described in the text.

DEM scheme (which requires the numerical solution of a system of coupled differential equations) is numerically close to an (explicit and faster) optical potential approximation (which requires a single computation only) suitable for inversion (see Johansen *et al.* 2002).

We all agree that a real shale should be treated as a $(\Phi_s + 1)$-phase material, where Φ_s represents the number of silt phases and the remaining phase is obviously represented by the randomly oriented crystals discussed earlier. To model this, we propose that one could let $C^{(0)}$ represent the overall properties of the less perfect shale (constructed using the CPA on the aggregate of randomly oriented spherical units of the perfect shale) and then estimate the effects of perturbations on this structure on the basis of the OPA, eq. (71), in conjunction with the numerical method for averaging over the inclusion orientations associated with eqs (80), (81) and (95). To a certain degree, this use of (a symmetric but non-self-consistent approximation) a less perfect shale (not involving silt) as the homogeneous reference medium takes into account the fact that the clay phase is connected and the silt phases are not. At the same time, the interactions between two inclusions only (e.g. silt–silt, silt–crystal, crystal–silt, crystal–crystal) are accounted for in the best possible manner. By not assuming that the spatial distributions of inclusions are (spherically symmetric) the same for all inclusion pairs, one may even mimic the behaviour of shales with microlayering or narrow bands of silt particles. Jakobsen & Johansen (2000) have published pictures of such complex media, showing sedimentary structures at the microscopic level.

Alternatively, one could also try to estimate the overall properties of a real shale on the basis of the generalized self-consistent condition (75), in conjunction with the numerical method for averaging over the orientations discussed earlier. However, the silt concentration should then probably not be larger than 40 per cent or so (because the silt may then become connected; Hornby *et al.* 1994), unless we are dealing with something more like a siltstone, where the silt is connected and the clay is not. These kinds of considerations represent our attempt to identify the most essential morphological features of shales. As a result of the complexity of the systems we are modelling, it is difficult to be sure what numerical scheme will work best in practice. A comparison between theoretical predictions and experimental data may help us to find out.

Let us now try to model small deformations and waves in the Jurassic shale of Hornby (1998); that is, to analyse the perhaps most complete data set published to date. The mineralogy is given in Table 1 (column 2), the density of the solid fraction is equal to 2680 kg m^{-3}, and the fluid-filled porosity is equal to 9.2 per cent (at 20 MPa hydrostatic pressure and pore fluid drained to atmosphere.) For each mineral

type and the fluid, the associated bulk and shear moduli are given in Table 1 (columns 3 and 4). Again, we have used a shale texture orientation distribution function having a Gaussian shape with a standard deviation of $\pi/9$.

Table 2 shows a comparison of theoretical predictions and experimental results for the effective stiffness constants, the vertical wave speeds and the anisotropy parameters of Thomsen (1986) (see also Tsvankin 1996). It appears that both the OPA- and the CPA-based models (based on the assumption that all two-point correlation functions are isotropic) can match the experimental value that Hornby (1998) recovered for the critical δ-parameter, which determines the shape of the wave fronts. All models correctly predict that $(\epsilon - \delta) > 0$, which means that the so-called anellipticity is positive, in the sense that the qP-wave slowness curve bulges out from the ellipse connecting the vertical and horizontal P-wave slownesses, and that the qSV-wave slowness curve is pushed inwards from the circle that connects its horizontal and vertical slownesses. (A positive anellipticity is commonly seen in shale acoustics (e.g. Hornby 1998; Jakobsen & Johansen 1999, 2000).) When it comes to the vertical wave speeds and the other Thomsen parameters, it appears that the OPA-based (CPA-based) model works best for the S waves (P waves). For these same quantities, it appears that the DEM-based model of Hornby *et al.* (1994) does not work satisfactorily for any type of wave. (Since we have analysed a single data set only, one should perhaps not infer too much from these observations.)

The rows in Table 2 labelled OPA* and CPA* are associated with two-point correlation functions that are lacking spherical symmetry (because we assumed that $\alpha_d^{(\rho\sigma)} = 0.1$ when $\rho = \sigma$ and $\alpha_d^{(\rho\sigma)} = 10$ when $\rho \neq \sigma$, where $\rho, \sigma = 1, \ldots, N_s + 1 = 6$), and have (in conjunction with the rows in Table 2 labelled OPA and CPA) a value in providing us with a kind of estimate of the uncertainty (associated with the unknown spatial distributions) in the predicted results for the elastic properties of a real shale without cracks.

8.4 The effect of cracks

Cracks in shales are not necessarily so large that it is obvious what homogeneous reference medium should be used when estimating the response of a single crack under a known stress field at infinity; the cracks may also be quite small and located between (or even within) the minerals within the shale. In addition, let us note that the treatment of real shales discussed in the previous subsection ignores the weaker bonding and greater compliance likely to exist at the edges of the individual domains of preferential particle alignment (see Bennett *et al.* 1991). This is probably a minor limitation which our model shares with all others published to date. If not, it can perhaps be compensated for by the introduction of a set of flat compliant cavities (a kind of crack) having orientations correlated with those of the randomly oriented crystals discussed earlier. From the discussion following eq. (87), however, it is clear that the computations will be rather involved.

For simplicity, we assume here that the scale-size of the cracks we are dealing with is much larger than those of the silt minerals, so that it makes sense to let $\boldsymbol{C}^{(0)}$ represent the effective properties of the real shale considered in the previous subsection, when estimating the overall properties of the cracked shale on the basis of the T-matrix theory. In addition, we restrict ourselves to cracks having normals along the main axis of symmetry for the TI shale. As a result, our cracked shale will still be characterized by a cylindrically symmetric microstructure. (Cracked shales may also behave elastically as a medium of orthorombic symmetry, provided that the crack normals are lying in the basal plane of the uncracked shale of hexagonal symmetry.)

In Fig. 4, the optical potential (Castaneda–Willis) approximation from eq. (73) behaves in a physically satisfactory manner at all crack densities investigated. This is in contrast with the behaviour of its second-order approximation from eq. (74), which shows an unphysical increase of effective stiffnesses with increasing crack density, when the crack density is larger than 0.1 or so. In the light of the fact that the second-order approximation in eq. (74) is consistent with the one that Hudson (1980, 1981) obtained on the basis of the method of smoothing (see Appendix C), this unphysical behaviour is not surprising (see Cheng 1993). The trouble starts when the second-order correction becomes larger than the corresponding first-order correction. To understand what is going on here, one must bear in mind that the Hudson-consistent expansion in terms of small crack density is an asymptotic expansion (with alternating signs). As emphasized by Cheng (1993), this means that the Hudson-consistent (direct T-matrix) expansion is approaching the true solution faster for the second-order than for the first-order expansion as the crack density approaches zero. It does not guarantee that the second-order approximations at higher crack densities are better than the

Table 2. Modelling shales without cracks: input mineralogy and porosity data, and elastic constants (measured at 20 MPa confining pressure) were found in the thesis of Hornby (1994). We have employed a Gaussian 'crystal' orientation distribution function having a standard deviation of $\pi/9$. OPA/CPA (OPA*/CPA*) refers to an optical/coherent potential approximation where all the correlation functions are isotropic (anisotropic). The differential effective medium (DEM) approximation was only used in conjunction with the shale model of Hornby *et al.* (1994). Stiffness constants are given in GPa and velocities V_p and V_s in m s^{-1}. ϵ, γ and δ are the dimensionless anisotropy parameters of Thomsen (1986).

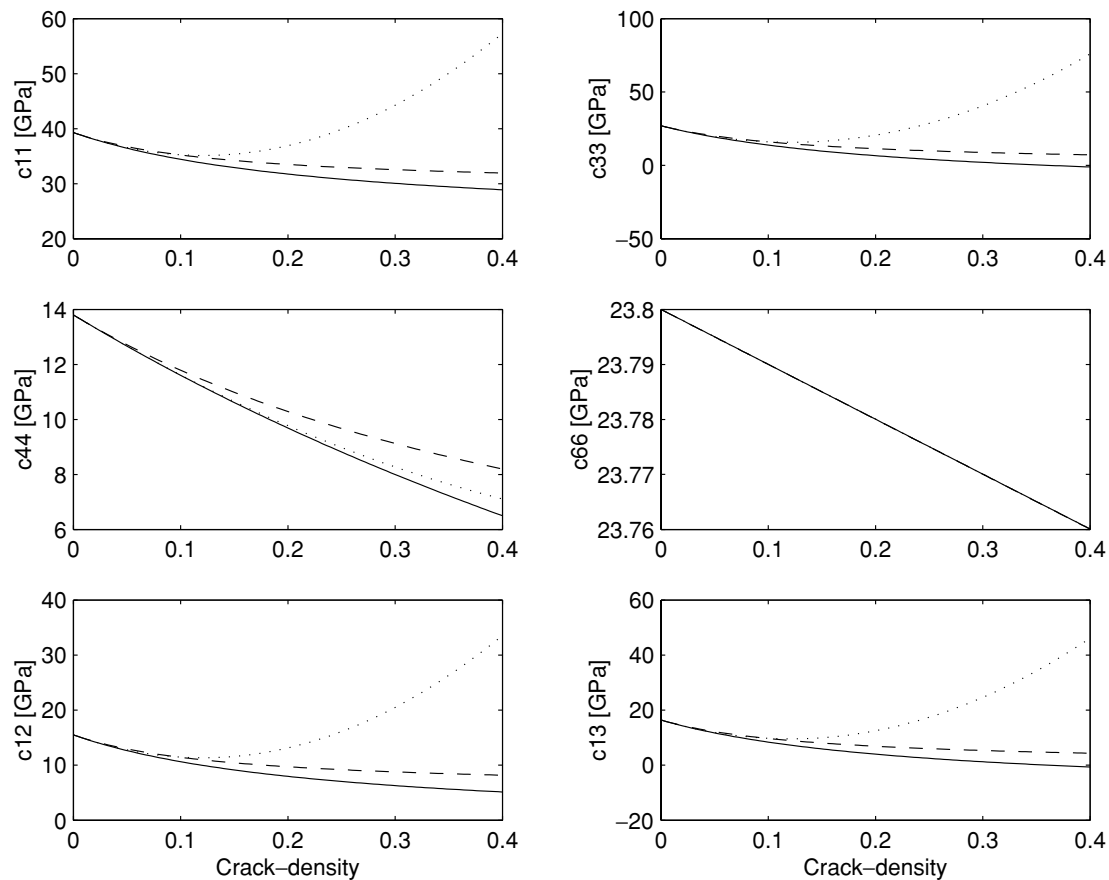|	c_{11}	c_{33}	c_{55}	c_{66}	c_{13}	V_p	V_s	ϵ	γ	δ
Data	39.3	27.0	6.9	11.9	16.4	3296	1660	0.23	0.37	0.12
OPA	35.9	21.3	6.7	11.8	10.3	2920	1633	0.34	0.39	0.12
CPA	40.2	25.8	8.9	13.8	10.8	3214	1892	0.28	0.27	0.12
DEM	28.4	17.9	3.4	7.8	11.8	2661	1167	0.30	0.64	0.04
OPA*	33.9	25.6	9.8	10.7	11.6	3196	1985	0.16	0.05	0.26
CPA*	38.9	25.7	9.3	13.1	10.9	3209	1925	0.26	0.21	0.16

Figure 4. The effective elastic stiffnesses of a real shale (data column, Table 3) containing two different spatial distributions of dry spheroidal cracks having an aspect ratio of 1/1000 and crack normals along the main symmetry axis of the shale. We have used the higher-order approximation (73) when the correlation function is isotropic (solid curves) and anisotropic (dashed curves). (The aspect ratio characterizing the ellipsoidal symmetry of the anisotropic correlation function was taken to be equal to the aspect ratio characterizing the shape of the cracks.) The dotted curves shows the predictions of the second-order approximation (74) when the correlation function is isotropic.

first-order approximations (Cheng 1993). When the crack density is no longer small, the Castaneda–Willis consistent T-matrix approximations (but definitely not their Hudson-consistent second-order approximations) may sometimes be close to the true solution.

The plots in Fig. 5 are based on the more general optical potential (non-self-consistent) approximation in eq. (71), and have value in demonstrating the importance of taking into account the effects of the spatial distribution when trying to deal with non-dilute mixtures of highly contrasting material properties. Using the results in Appendix C, one could investigate similar phenomena on the basis of a combination of the T-matrix approach with Hudson's familiar (crack model) displacement discontinuity parameters.

9 CONCLUDING REMARKS

In this work, integral equation methods (Green's function techniques) have been used to obtain new estimates of the effective stiffness tensors for a wide range of shale-related media with inclusions that are either embedded in a homogeneous matrix material or else make up a granular aggregate. Specifically, the T-matrix formalism of Zeller & Dederichs (1973) (which operates with an arbitrary homogeneous reference medium) was adopted for complex microstructures with prescribed two-point correlation functions for the statistics of centres of arbitrarily shaped inclusions (solid particles or fluid-filled cavities). When the inclusions are not only ellipsoidal in shape but also distributed in space in accordance with two-point correlation functions having ellipsoidal symmetries, completely explicit expressions for the effective stiffness tensors are obtained in terms of fourth-rank tensors serving to characterize the shapes/orientations of the inclusions, and other fourth-rank tensors associated with their spatial distributions. If the aspect ratios of the correlation functions (that can be selected independently from those of the inclusions) are taken to be the same for all pairs of interacting inclusions (although this is not required), the Hashin–Strikman-type approximation that Ponte Castaneda & Willis (1995) derived on the basis of the variational method is recovered, provided that the matrix material itself is used as the reference medium. If the Castaneda–Willis approximation is expanded to second order in the inclusion concentrations (or crack densities), the popular theories (or crack models) that Hudson (1980, 1981, 1988, 1994a,b) derived on the basis of the method of smoothing can also be recovered, provided that all correlation functions are taken to be isotropic. We have seen that the Castaneda–Willis-consistent T-matrix approximations (having the same form as an exact formal solution in terms of the ensemble-averaged
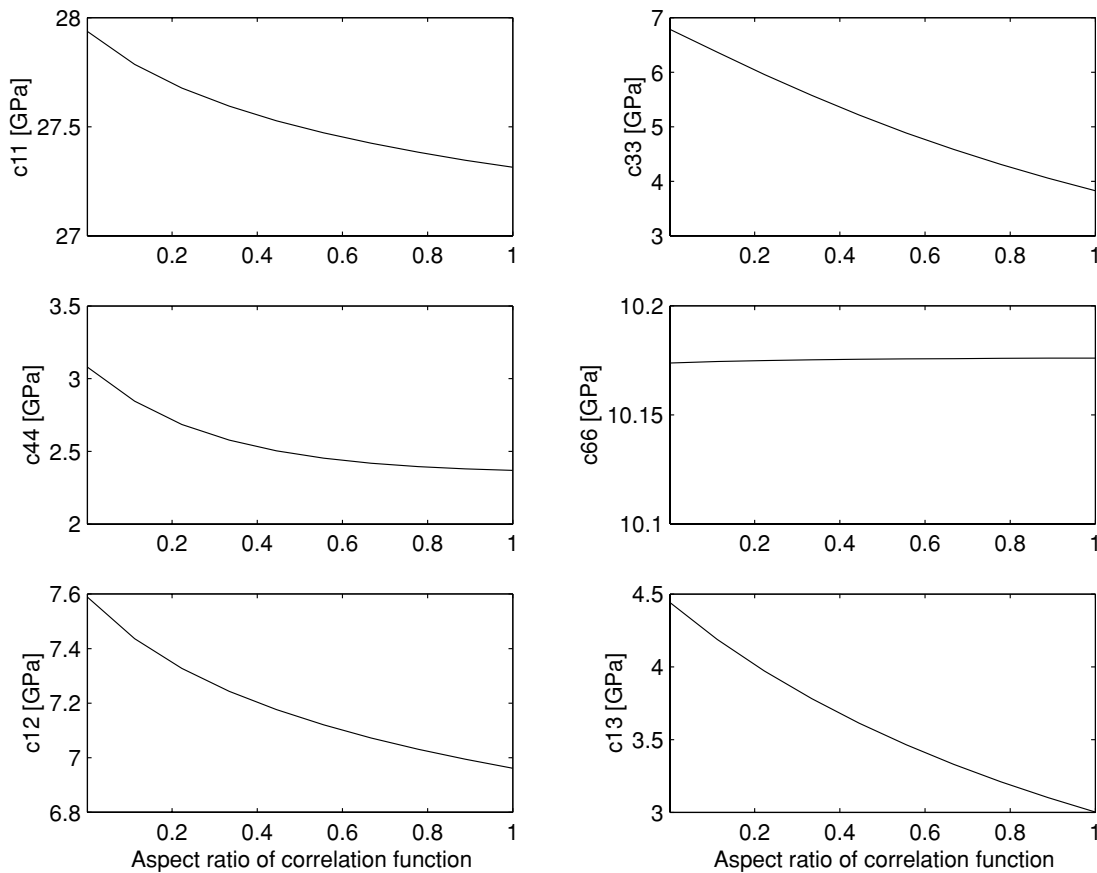
Figure 5. The same shale matrix as in Fig. 5 is here containing two different crack sets, labelled by $i = 1, 2$. We ensured that $\alpha^{(1)} = 0.1$, $\alpha^{(2)} = 0.001$ and $v^{(1)} = 0.1257$, $v^{(2)} = 0.0013$, where $\alpha^{(i)}$ and $v^{(i)}$ refers to the aspect ratio and volume concentration, respectively. In this numerical experiment, cracks of type 1 are water-filled, and cracks of type 2 are dry. We took $\alpha_d^{(11)} = \alpha^{(1)}$ and $\alpha_d^{(22)} = \alpha^{(2)}$. Aspect ratio of correlation function means $\alpha_d^{(12)} = \alpha_d^{(21)}$, where $\alpha_d^{(12)}$ is associated with $p^{(1|2)}$, etc. The smallest aspect ratio of correlation function is equal to $\alpha^{(2)}$ in this case.

T-matrix for the material, which satisfies an integral equation of the Lippmann–Schwinger type) virtually always produces results that are physically plausible, but their Hudson-consistent second-order approximations predict unphysical turning points at relatively low inclusion concentrations (or crack densities). Therefore, we recommend using the Castaneda–Willis-consistent T-matrix approximations, unless the inclusion concentrations are dilute. (A 'non-dilute version' of Hudson's simple model for cracked isotropic media appeared in (Appendix C) the form of a new combination of the familiar displacement discontinuity parameters of Hudson with the Castaneda–Willis-consistent T-matrix approximations.) It is an important feature of the T-matrix approach that it operates with an arbitrary reference medium, since the whole issue of effective medium theory in many ways appears to be a search for the most suitable comparison material. For shale-related materials without a well-defined matrix material, it may sometimes be a good idea to let the effective medium itself be the reference medium. In this way, we obtained generalized self-consistent estimates (from the Castaneda–Willis-consistent T-matrix approximations) that explicitly take into account the interaction between two inclusions only. If and only if the spatial distribution is taken to be the same for all pairs of interacting inclusions, the self-consistent approximation of Hornby *et al.* (1994) recovered.

Overall, the 'T-matrix approach to shale acoustics' may be regarded as a 'modern' counterpoint to the work of Hornby *et al.* (1994), which emphasizes the uncertainties inherent in that approach, and defines a direction for further theoretical developments. When we first realized that the T-matrix formalism (analogous to quantum mechanical multiple-scattering theory) could do more than just re-derive virtually all existing theories of shale-related composites, we initially become very optimistic about the prospects of arriving at a reliable tool for seismic analysis in shale formations. However, as soon as we started to investigate the predictions of the various approximations that make up our new hierarchy of increasingly realistic models for shales (that have been examined under the microscope), we quickly become less optimistic (if not pessimistic). Even for perfect shales (treated as fully aligned clay–fluid composites) there appear to exist several different modelling procedures that are more or less equally plausible but produce markedly different results. The simple Hill approximation that Hornby *et al.* used to (average over the orientations) construct a (polycrystal) less perfect shale may be accurate enough on its own, but scaling arguments suggest one should perhaps average over the orientations simultaneously as one adds silt (if the goal is to model real shales as seen in the laboratory). We have found that this can be done (with different results) on the basis of generalized self-consistent (coherent potential) as well as non-self-consistent (optical potential) approximations, but it is important to ensure that the silt inclusions (building blocks) are unconnected (connected). It is an unfortunate feature that the theoretical predictions are rather sensitive to the assumptions one makes concerning the

spatial distributions, because these are rarely known with high confidence. Under the assumption that all correlation functions are isotropic, models based on the T-matrix approach (not involving the DEM scheme at any stage) performed better than the model of Hornby *et al.* (1994) (involving the DEM scheme at two stages). However, the match between theory and experiment was never completely satisfactory. Our theoretical modelling suggests that a small number of aligned cracks in anisotropic shales can dramatically increase the overall anisotropy, and so (when it comes to the analysis of experimental data) it is important to bear in mind that such cracks can be created during man-made as well as natural processes. Despite all of this, we see no reason for creating an atmosphere of hopelessness. Further progress in theoretical shale acoustics may be obtained if the experimentalists can help us to find out what theoretical possibilities work best in practice, and come up with a more quantitative description of the microstructures of (cracked) shales as seen in the laboratory. It would also be helpful if more experiments on the (anisotropic) elastic properties of pure clay minerals could be performed along the lines of Katahara (1996) and Wang *et al.* (2001).

Finally, it may be noted that the activity reported here is part of a larger programme focusing on the development of inclusion-based models for porous/cracked rocks of interest to the petroleum industry. Recent developments suggest that it is possible to use the T-matrix approach to formulate a unified theory of rocks as viscoelastic composites. Jakobsen *et al.* (2002) have, for example, derived a novel expression for the t-matrix of a communicating cavity; that is, a fully fluid-saturated cavity which may exchange fluid mass with other cavities due to local and/or global fluid pressure gradients, caused by the passage of a relatively long acoustic wave. (Since shales are normally characterized by an extremely low permeability, we assumed in this paper that cavities in shales are isolated with respect to fluid flow.) In order to arrive at a general tool for seismic reservoir characterization, we probably need to make the T-matrix theory fully dynamic, so that it can take into account the multiple-scattering phenomenon associated with the transport of energy out of the coherent wave and into the coda. This has of course nothing to do with the energy dissipation phenomenon associated with communicating cavities, but both phenomena may sometimes occur simultaneously (if the frequency is sufficiently large), and so there is plenty of space for more work along these lines, which are not restricted to isotropic media in any sense.

ACKNOWLEDGMENTS

REFERENCES

Auld, B.A., 1990. *Acoustic Fields and Waves in Solids,* Krieger, Malabar.

Bennett, R.H., Bryant, W.R. & Hulbert, M.H., 1991. *Microstructure of Fine-Grained Sediments: From Mud to Shale,* Springer-Verlag, New York.

Berryman, J.G., 1980a. Long-wavelength propagation in composite elastic media I: spherical inclusions, *J. acoust. Soc. Am.,* **68,** 1809–1819.

Berryman, J.G., 1980b. Long-wavelength propagation in composite elastic media II: ellipsoidal inclusions, *J. acoust. Soc. Am.,* **68,** 1820–1831.

Berryman, J.G., 1992. Single-scattering approximations for coefficients in Biot's equations of poroelasticity, *J. acoust. Soc. Am.,* **91,** 551–570.

Budiansky, B., 1965. On the elastic moduli of some heterogeneous materials, *J. Mech. Phys. Solids.,* **13,** 223–227.

Bunge, H.J., 1974. Mittelungsverfahren bei dreidimensionalen texturen, in *Mechaniche Anisotropie,* pp. 177–199, ed. Stuwe, H.P., Wien, Springer-Verlag.

Cheng, C.H., 1993. Crack models for a transversely isotropic medium, *J. geophys. Res.,* **98,** 675–684.

Christensen, R.M., 1976. *Mechanics of Composite Materials,* Wiley, New York.

Dederich, P.H. & Zeller, R., 1972. Elastische konstanten von vielkristallen, Report Jul-877-FF.

Diz, J. & Humbert, M., 1992. Practical aspects of calculating the elastic properties of polycrystals from the texture according to different models, *J. Appl. Cryst.,* **25,** 756–760.

Domany, E., Gubernatis, J.E. & Krumhansl, J.A., 1975. The elasticity of polycrystals and rocks, *J. geophys. Res.,* **80,** 4851–4856.

Douma, J., 1988. The effect of the aspect ratio on cracked-induced anisotropy, *Geophys. Prospect.,* **36,** 614–632.

Elliott, R.J., Krumhansl, J.A. & Leath, P.L., 1974. The theory and properties of randomly disordered crystals and related physical systems, *Rev. Mod. Phys.,* **46,** 465–542.

Eshelby, J.D., 1957. The determination of the elastic field of an ellipsoidal inclusion, and related problems, *Proc. R. Soc. Lond.,* A., **241,** 376–396.

Gibson, R.L. & Toksoz, M.N., 1990. Permeability estimation from velocity anisotropy in fractured rock, *J. geophys. Res.,* **95,** 15 643–15 655.

Goldberger, M.L. & Watson, K.M., 1964. *Collision Theory,* Wiley, New York.

Gubernatis, J.E. & Krumhansl, J.A., 1975. Macroscopic engineering properties of polycrystalline materials: elastic properties, *J. Appl. Phys.,* **46,** 1875–1883.

Gueguen, Y., Chelidze, T. & Ravalec, M.L., 1997. Microstructures, percolation thresholds, and rock physical properties, *Tectonophysics,* **279,** 23–35.

Hendrix, B.C. & Yu, L.G., 1998. Self-consistent elastic properties for transversely isotropic polycrystals, *Acta mater.,* **46,** 127–135.

Hershey, A.V., 1954. The elasticity of an isotropic aggregate of anisotropic crystals, *J. Appl. Mech.,* **21,** 236–240.

Hill, R., 1952. The elastic behaviour of a crystalline aggregate, *Proc. Phys. Soc. Lond.*, A., **65,** 349–354.

Hill, R., 1965. A self-consistent mechanics of composite materials, *J. Mech. Phys. Solids,* **13,** 213–222.

Hirsekorn, S., 1990. Elastic properties of polycrystals: a review, *Textures Microstructures,* **12,** 1–14.

Hornby, B.E., 1994. The Elastic Properties of Shales, *PhD thesis*, Univ. Cambridge.

Hornby, B.E., 1998. Experimental laboratory determination of the dynamic elastic properties of wet, drained shales, *J. geophys. Res.,* **103,** 29 945–29 964.

Hornby, B.E., 2001. Upscaling: elastic anisotropy from ultrasonic laboratory measurements to borehole seismic surveys, in *Advances in Anisotropy: Selected Theory, Modeling, and Case Studies, Proc. 7th Int. Workshop on Seismic Anisotropy (7IWSA)*, ed. Julie A. Hood, Society of Exploration Geophysics (SEG).

Hornby, B.E., Schwartz, L.M. & Hudson, J.A., 1994. Anisotropic effective medium modeling of the elastic properties of shales, *Geophysics,* **59,** 1570–1583.

Hudson, J.A., 1980. Overall properties of a cracked solid, *Math. Proc. Camb. Phil. Soc.,* **88,** 371–384.

Hudson, J.A., 1981. Wave speeds and attenuation of elastic waves in material containing cracks, *Geophys. J. R. astr. Soc.,* **87,** 265–274.

Hudson, J.A., 1988. Seismic wave propagation through material containing partially saturated cracks, *Geophys. J.,* **92,** 33–37.

Hudson, J.A., 1991. Overall properties of heterogeneous material, *Geophys. J. Int.,* **107,** 505–511.

Hudson, J.A., 1994a. Overall properties of a material with inclusions or cavities, *Geophys. J. Int.,* **117,** 555–561.

Hudson, J.A., 1994b. Overall properties of anisotropic materials containing cracks, *Geophys. J. Int.,* **116,** 279–282.

Hudson, J.A., Liu, E. & Crampin, S., 1996. The mechanical properties of materials with interconnected cracks and pores, *Geophys. J. Int.,* **124,** 105–112.

Humbert, M., Wagner, F., Philippe, M.J. & Esling, C., 1991. Relations between texture and anisotropic properties: some applications to low symmetry materials, *Textures Microstructures,* **14–18,** 443–461.

Jakobsen, M., 1998. Acoustics of complex porous media, *PhD thesis,* Univ. Bergen.

Jakobsen, M. & Johansen, T.A., 1999. A test of ANNIE based on ultrasonic measurements on a shale, *J. Seism. Expl.,* **8,** 77–89.

Jakobsen, M. & Johansen, T.A., 2000. Anisotropic approximations for mudrocks: a seismic laboratory study, *Geophysics,* **65,** 1711–1725.

Jakobsen, M., Hudson, J.A., Minshull, T.A. & Singh, S.C., 2000. Elastic properties of hydrate-bearing sediments using effective medium theory, *J. geophys. Res.,* **105,** 561–577.

Jakobsen, M., Johansen, T.A. & McCann, C., 2003. The acoustic signature of fluid flow in complex porous media, *J. appl. Geophys.* in press

Jeffreys, H. & Jeffreys, B.S., 1972. *Methods of Mathematical Physics*, Cambridge Mathematical Library, Cambridge University Press, Cambridge.

Johansen, T.A., Ruud, B.O. & Jakobsen, M., 2000. Influence of the grain orientation distribution on the AVO of *PP* and *PS* waves, *62nd EAGE meeting,* Glasgow, extended abstracts I, C-40.

Johansen, T.A., Jakobsen, M. & Ruud, B.O., 2002. Estimation of the internal structure and anisotropy of shales from borehole data, *J. Seism. Expl.,* **11,** 363–381.

Johansen, T.A., Ruud, B.O. & Jakobsen, M., 2003. Effects of grain scale alignment on seismic anisotropy and reflectivity of shales, *Geophys. Prosp.* submitted.

Johnston, D.H., 1987. Physical properties of shale at temperature and pressure, *Geophysics,* **10,** 1391–1401.

Johnston, J.E. & Christensen, N.I., 1995. Seismic anisotropy of shales, *J. geophys. Res.,* **B4,** 5991–6003.

Jones, L.E.A. & Wang, H.F., 1981. Ultrasonic velocities in Cretaceous shales from the Williston Basin, *Geophysics,* **46,** 288–297.

Kaarsberg, E.A., 1959. Introductory studies of natural and artificial argillaceous aggregates by sound-propagation and X-ray diffraction methods, *J. Geol.,* **67,** 447–472.

Kachanov, M., 1993. Elastic solids with many cracks and related problems, *Adv. Appl. Mech.,* **30,** 259–445.

Katahara, K.W., 1996. Clay mineral elastic properties, *66th SEG Meeting,* Denver, Extended abstracts II, pp. 1691–1694.

Keller, J.B., 1964. Stochastic equations and wave propagation in random media, *Proc. Symp. appl. Math.,* **16,** 145–170.

Kelvin, Lord (Thomson, W.), 1856. Elements of a mathematical theory of elasticity, part 1 On stresses and strains, *Phil. Trans. R. Soc. Lond.*, A., **166,** 481–498.

Korringa, J., 1979. Multiple scattering theory and the self-consistent imbedding approximation, in *Acoustic, Electromagnetic and Elastic Wave Scattering—Focus on the T-matrix Approach, Proc. Int. Symp. held at The Ohio State University*, pp. 529–535, eds Varadan, V.K. & Varadan, V.V.

Kroner, E., 1958. Berechnung der elastischen konstanten des vielkristalls aus den konstanten des einkristalls, *Z. Phys.,* **151,** 504–518.

Kroner, E., 1986. Statistical modelling, in *Modelling Small Deformations of Polycrystals*, pp. 229–291, eds Gittus, J. & Zarka, J., Elsevier, London.

Lo, T.W., Coyner, K.B. & Toksoz, M.N., 1986. Experimental determination of elastic anisotropy of Berea sandstone, Chicopee shale and Chelmsford granite, *Geophysics,* **51,** 164–171.

McCoy, J.J., 1979. On the calculation of bulk material properties of heterogeneous materials, *Q. Appl. Math.*, July, 137–149.

Mainprice, D., 1997. Modelling the anisotropic seismic properties of partially molten rocks found at mid-ocean ridges, *Tectonophysics,* **279,** 161–179.

Mainprice, D. & Humbert, M., 1994. Methods for calculating petrophysical properties from lattice preferred orientation data, Surveys in *Geophysics,* **15,** 575–592.

March, N.H., Young, W.H. & Sampanthar, S., 1967. *The Many-body Problem in Quantum Mechanics,* Dover, New York.

Middya, T.R. & Basu, A.N., 1986. Self-consistent *T*-matrix solution for the effective elastic properties of noncubic polycrystals, *J. Appl. Phys.,* **59,** 2368–2375.

Molinari, A. & Mouden, M.E., 1996. The problem of elastic inclusions at finite concentrations, *Int. J. Solids Structures,* **33,** 3131–3150.

Morris, P.R., 1969. Averaging fourth-rank tensors with weight functions, *J. Appl. Phys.,* **40,** 447–448.

Morris, P.R., 1970. Elastic constants of polycrystals, *Int. J. Eng. Sci.,* **8,** 49–61.

Mura, T., 1982. *Micromechanics of Defects in Solids,* Nijhoff, Zoetermeer.

Musgrave, M.J.P., 1970. *Crystal Acoustics,* Holden Day, San Francisco.

Nan, C.W., Birringer, R. & Gleiter, H., 1998. On correlation effect in *t*-matrix method for effective elastic moduli of composites, *Phys. Stat. Sol. (b),* **205,** R9–R10.

Nemat-Nasser, S. & Hori, M., 1993. *Micromechanics: Overall Properties of Heterogeneous Materials,* North-Holland, New York.

Nishizawa, O., 1982. Seismic velocity anisotropy in a medium containing oriented cracks—transversely isotropic case, *J. Phys. Earth,* **30,** 331–347.

Nowick, S.A., 1995. *Crystal Properties via Group Theory,* Cambridge University Press, Cambridge.

Podio, A.L., Gregory, A.R. & Grey, M.E., 1968. Dynamic properties of dry and water-saturated Green River shale under stress, *Soc. Ptr. Eng. J.,* **8,** 389–404.

Ponte Castaneda, P. & Willis, J.R., 1995. The effect of spatial distribution on the effective behaviour of composite materials and cracked media, *J. Mech. Phys. Solids,* **43,** 1919–1951.

Reuss, A., 1929. Berechnung der Fliessgrenze von Mischkristallen auf Grund der Plastizitatbedingung für einkristale, *Z. Ang. Math. Mech.,* **9,** 49.

Roach, G.F., 1999. *Green's Functions*, Cambridge University Press, Cambridge.

Roe, R.J., 1965. Description of crystallite orientation in polycrystalline materials. III. General solution to pole figure inversion, *J. Appl. Phys.,* **36,** 2024–2031.

Sams, M.S. & Andrea, M., 2001. The effect of clay distribution on the elastic properties of sandstones, *Geophys. Prospect.,* **49,** 128–150.

Sarkar, S., Ballabh, T.K., Middya, T.R. & Basu, A.N., 1996. *T*-matrix approach to effective nonlinear elastic constants of heterogeneous materials, *Phys. Rev.,* **54,** 3926–3931.

Sayers, C.M., 1994. The elastic anisotropy of shales, *J. geophys. Res.,* **99,** 767–774.

Sayers, C.M., 1999. Stress-dependent seismic anisotropy of shales, *Geophysics,* **59,** 93–98.

Sherwood, J.D., 1993. Biot poroelasticity of a chemically active shale, *Proc. R. Soc. Lond.,* A., **440,** 365–377.

Sheng, P., 1990. Effective-medium theory of sedimentary rocks, *Phys. Rev. B,* **41,** 4507–4512.

Sisodia, P. & Verma, M.P., 1990. Polycrytalline elastic moduli of some hexagonal and tetragonal materials, *Phys. Stat. Sol. (a),* **122,** 525–533.

Soven, P., 1967. Coherent-potential model of substitutional disordered alloys, *Phys. Rev.,* **156,** 809–813.

Taylor, D.W., 1967. Vibrational properties of imperfect crystals with large defect concentrations, *Phys. Rev.,* **156,** 1017–1029.

Thomsen, L., 1972. Elasticity of polycrystals and rocks, *J. geophys. Res.,* **77,** 315–327.

Thomsen, L., 1985. Biot-consistent elastic moduli of porous rocks: low-frequency limit, *Geophysics,* **50,** 2797–2807.

Thomsen, L., 1986. Weak elastic anisotropy, *Geophysics,* **51,** 1954–1966.

Torquato, S., 1998. Exact expression for the effective elastic tensor of disordered composites, *Phys. Rev. Lett.,* **79,** 681–684.

Tsvankin, I., 1996. *P*-wave signatures and notation for transversely isotropic media: an overview, *Geophysics,* **61,** 467–483.

Vernik, L., 1994. Hydrocarbon-generation-induced microcracking of source rocks, *Geophysics,* **59,** 555–563.

Vernik, L. & Liu, X., 1997. Velocity anisotropy in shales: a petrophysical study, *Geophysics,* **62,** 521–532.

Voigt, W., 1887. Theoretische Studien uber die Elastizitatverhaltnisse der Krystalle, *Abh. Kgl. Ges. Wiss. Gottingen, Math. Kl.,* **34,** l, in part, p. 47 ff.

Wang, Z., Wang, H. & Cates, M.E., 2001. Effective elastic properties of solid clays, *Geophysics,* **66,** 428–440.

Watson, K.M., 1957. Multiple scattering by quantum-mechanical systems, *Phys. Rev.,* **105,** 1388–1398.

Weyl, H., 1957. *Theory of Groups and Quantum Mechanics,* Dover, New York.

White, J.E., Martineau-Nicoletis, L. & Monash, C., 1983. Measured anisotropy in Pierre shale, *Geophys. Prospect.,* **31,** 709–725.

Winterstein, D.F. & Paulson, B.N.P., 1990. Velocity anisotropy in shale determined from cross-hole seismic and VSP data, *Geophysics,* **55,** 470–479.

Willis, J.R., 1977. Bounds and self-consistent estimates for the overall properties of anisotropic composites, *J. Mech. Phys. Solids,* **25,** 185–202.

Willis, J.R., 1981. Variational and related methods for the overall properties of composites, *AdV. Appl. Mech.,* **21,** 1–78.

Xu, S., 1998. Modelling the effect of fluid communication on velocities in anisotropic porous rocks, *Int. J. Solids Structures.,* **35,** 4685–4707.

Yin, H., 1993. Acoustic velocity and attenuation in rocks: isotropy, intrinsic anisotropy, and stress induced anisotropy, *PhD thesis,* Stanford University.

Zeller, R. & Dederichs, P.H., 1973. Elastic constants of polycrystals, *Phys. Stat. Sol. (b),* **55,** 831–843.

APPENDIX A: INTEGRAL OPERATOR ALGEBRA

Eq. (28) may be written in operator notation as

$$\boldsymbol{T}_\alpha^{(r)} = \delta \boldsymbol{C}_\alpha^{(r)} + \delta \boldsymbol{C}_\alpha^{(r)} \mathcal{G} \sum_{s,\beta} \boldsymbol{T}_{\beta,}^{(s)} \tag{A1}$$

or

$$\left(\mathcal{I} - \delta \boldsymbol{C}_\alpha^{(r)} \mathcal{G}\right) \boldsymbol{T}_\alpha^{(r)} = \delta \boldsymbol{C}_\alpha^{(r)} + \delta \boldsymbol{C}_\alpha^{(r)} \mathcal{G} \sum_{s,\beta} \boldsymbol{T}_\beta^{(s)} (1 - \delta_{rs} \delta_{\alpha\beta}). \tag{A2}$$

The operators $\mathcal{I}$ and $\mathcal{G}$ are defined by

$$[\mathcal{I}\mathbf{A}](\mathbf{x}) = \int_\Omega d\mathbf{x}' \boldsymbol{I} \delta(\mathbf{x} - \mathbf{x}') \mathbf{A}(\mathbf{x}'), \tag{A3}$$

$$[\mathcal{G}\mathbf{A}](\mathbf{x}) = \int_\Omega d\mathbf{x}' \boldsymbol{G}^{(0)}(\mathbf{x} - \mathbf{x}') \mathbf{A}(\mathbf{x}'), \tag{A4}$$

where $\mathbf{A}(\mathbf{x})$ is any fourth-rank tensor field. Operating equation (A2) with $(\mathcal{I} - \delta \boldsymbol{C}_\alpha^{(r)} \mathcal{G})^{-1}$ from the left, we obtain

$$\boldsymbol{T}_\alpha^{(r)} = \boldsymbol{t}_\alpha^{(r)} + \boldsymbol{t}_\alpha^{(r)} \mathcal{G} \sum_{s,\beta} \boldsymbol{T}_\beta^{(s)} (1 - \delta_{rs} \delta_{\alpha\beta}), \tag{A5}$$

where

$$\boldsymbol{t}_\alpha^{(r)} = \left(\mathcal{I} - \delta \boldsymbol{C}_\alpha^{(r)} \mathcal{G}\right)^{-1} \delta \boldsymbol{C}_\alpha^{(r)} \tag{A6}$$

is the solution to the integral equation

$$\boldsymbol{t}_\alpha^{(r)} = \delta \boldsymbol{C}_\alpha^{(r)} + \delta \boldsymbol{C}_\alpha^{(r)} \mathcal{G} \boldsymbol{t}_\alpha^{(r)}. \tag{A7}$$

We note that $\mathcal{G}$ may be treated formally as an operator in the Hilbert space with unity operator $\mathcal{I}$ (see Kroner 1986; Roach 1999). For concreteness, we have avoided all operator notation in the main text of this paper.

APPENDIX B: TWO-POINT STATISTICS

The characteristic function of phase *r* can be written as

$$\bar{\theta}^{(r)}(\mathbf{x}) = \int_\Omega d\mathbf{z} \theta^{(r)}(\mathbf{x} - \mathbf{z}) \phi^{(r)}(\mathbf{z}), \tag{B1}$$

where

$$\phi^{(r)}(\mathbf{z}) = \sum_{\alpha=1}^{n^{(r)}} \delta \left(\mathbf{z} - \mathbf{x}_\alpha^{(r)} \right), \tag{B2}$$

is the random density field generated by the set of random points $\mathbf{x}_\alpha^{(r)}$ (Ponte Castaneda & Willis 1995). Eq. (67) and (B8) gives

$$\langle \mathbf{A}^{(rs)} \rangle = \int_\Omega d\mathbf{x}' \int_\Omega d\mathbf{z} \int_\Omega d\mathbf{z}' \, \mathbf{G}^{(0)}(\mathbf{x} - \mathbf{x}')\theta^{(r)}(\mathbf{x} - \mathbf{z})\theta^{(s)}(\mathbf{x}' - \mathbf{z}') \left[\langle \phi^{(r)}(\mathbf{z})\phi^{(s)}(\mathbf{z}') \rangle - \langle \phi^{(r)}(\mathbf{z})\rangle\langle\phi^{(s)}(\mathbf{z}') \rangle \right]. \tag{B3}$$

According to Ponte Castaneda & Willis (1995), we have

$$\langle \phi^{(r)}(\mathbf{z}) \rangle = p^{(r)}(\mathbf{z}), \tag{B4}$$

$$\langle \phi^{(r)}(\mathbf{z})\phi^{(s)}(\mathbf{z}') \rangle = \delta_{rs} p^{(r)}(\mathbf{z})\delta(\mathbf{z} - \mathbf{z}') + p^{(rs)}(\mathbf{z} - \mathbf{z}'), \tag{B5}$$

where $p^{(r)}(\mathbf{z})$ denotes the probability density for finding an inclusion of type r centred at $\mathbf{z}$, and $p^{(rs)}(\mathbf{z}, \mathbf{z}')$ correspondingly denotes the joint probability density for finding an inclusion of type r centred at $\mathbf{z}$ and an inclusion of type s centred at point $\mathbf{z}'$. Since the random medium is assumed to be statistically homogeneous, it is clear that $p^{(r)}(\mathbf{z}) = p^{(r)} = n^{(r)}/|\Omega|$, and $p^{(rs)}(\mathbf{z},\mathbf{z}') = p^{(rs)}(\mathbf{z} - \mathbf{z}')$. Eqs (B3)–(B5) imply that

$$\langle \mathbf{A}^{(rs)} \rangle = \int_\Omega d\mathbf{x}' \int_\Omega d\mathbf{z} \int_\Omega d\mathbf{z}' \, \mathbf{G}^{(0)}(\mathbf{x} - \mathbf{x}')\theta^{(r)}(\mathbf{x} - \mathbf{z})\theta^{(s)}(\mathbf{x}' - \mathbf{z}') \left[p^{(rs)}(\mathbf{z} - \mathbf{z}') - p^r p^s \right]$$
$$+ \delta_{rs} p^{(r)} \int_\Omega d\mathbf{x}' \int_\Omega d\mathbf{z} \, \mathbf{G}^{(0)}(\mathbf{x} - \mathbf{x}')\theta^{(r)}(\mathbf{x} - \mathbf{z})\theta^{(s)}(\mathbf{x}' - \mathbf{z}). \tag{B6}$$

In the rest of this appendix, we follow closely the derivations of Ponte Castaneda & Willis (1995). First we introduce two sets of new variables to evaluate the integrals on the right-hand side of eq. (B6). Specifically, we use the substitutions $\mathbf{y} = \mathbf{x} - \mathbf{z}$, $\mathbf{y}' = \mathbf{x}' - \mathbf{z}'$, $\mathbf{z}'' = \mathbf{z}' - \mathbf{z}$ in the first term, and $\mathbf{y} = \mathbf{x} - \mathbf{z}$, $\mathbf{y}' = \mathbf{x}' - \mathbf{z}$ in the second term. It follows that

$$\langle \mathbf{A}^{(rs)} \rangle = \int d\mathbf{y} \int d\mathbf{y}' \int d\mathbf{z}'' \, \mathbf{G}^{(0)}(\mathbf{y} - \mathbf{y}' - \mathbf{z}'')\theta^{(r)}(\mathbf{y})\theta^{(s)}(\mathbf{y}') \left[p^{(rs)}(\mathbf{z}'') - p^{(r)} p^{(s)} \right] + \delta_{rs} p^{(s)} \int d\mathbf{y} \int d\mathbf{y}' \, \mathbf{G}^{(0)}(\mathbf{y} - \mathbf{y}')\theta^{(r)}(\mathbf{y})\theta^{(s)}(\mathbf{y}'), \tag{B7}$$

where the integrals have been performed formally over all space, because their kernels ensure restrictions to finite domains for $\mathbf{y}$ and $\mathbf{y}'$, and decay of a small 'correlation length' for $\mathbf{z}''$. Eq. (B7) is equivalent to

$$\langle \mathbf{A}^{(rs)} \rangle = p^{(r)} \int_{\Omega^{(r)}} d\mathbf{y} \int_{\Omega^{(s)}} d\mathbf{y}' \int d\mathbf{z}'' \, \mathbf{G}^{(0)}(\mathbf{y} - \mathbf{y}' - \mathbf{z}'') \left[p^{(s|r)}(\mathbf{z}'') - p^{(s)} \right] + \delta_{rs} p^{(s)} \int_{\Omega^{(r)}} d\mathbf{y} \int_{\Omega^{(s)}} d\mathbf{y}' \, \mathbf{G}^{(0)}(\mathbf{y} - \mathbf{y}'), \tag{B8}$$

where $p^{(s|r)}(\mathbf{z}', \mathbf{z}) = p^{(rs)}(\mathbf{z}, \mathbf{z}')/p^{(r)}$ is the (translation-invariant) conditional probability density for finding an inclusion of type s centred at point $\mathbf{z}'$ given that there is an inclusion of type r centred at point $\mathbf{z}$. We note that $p^{(rs)}(\mathbf{z} - \mathbf{z}') = p^{(sr)}(\mathbf{z}' - \mathbf{z})$, which implies that $p^{(rs)}(\mathbf{z}'') = p^{(sr)}(-\mathbf{z}'')$. This, together with the fact that $\mathbf{G}^{(0)}(-\mathbf{x}) = \mathbf{G}^{(0)}(\mathbf{x})$, implies that $\langle \mathbf{A}^{(rs)} \rangle = \langle \mathbf{A}^{(sr)} \rangle$.

We now assume that $p^{(s|r)}$ depends on $\mathbf{z}''$ only through the combination $|\mathbf{Z}_d^{(rs)}\mathbf{z}''|$, where $\mathbf{Z}_d^{(rs)}$ is a 3×3 matrix which defines an ellipsoid;

$$\Omega_d^{(rs)} = \left\{ \text{all points } \mathbf{x} \text{ so that } \left| \mathbf{Z}_d^{(rs)} \cdot \mathbf{x} \right| < 1 \right\}, \tag{B9}$$

serving to characterize the spatial distribution of inclusions. Since $p^{(rs)}(\mathbf{z}'') = p^{(sr)}(-\mathbf{z}'')$ we must have that $\mathbf{Z}_d^{(rs)} = \mathbf{Z}_d^{(sr)}$ and $\Omega_d^{(rs)} = \Omega_d^{(sr)}$. We also assume that the inclusions do not overlap. Under the assumed symmetry for the two-point probability density function, this implies that $p^{(s|r)} = 0$ for $\mathbf{z}'' \in \Omega_d^{(rs)}$. We divide the integral with respect to $\mathbf{z}''$ in the first term on the right-hand side of eq. (B8) into two parts, the first part being an integral over $\Omega_d^{(rs)}$ and the second term an integral over the complement of $\Omega_d^{(rs)}$. With the above assumption for the statistical distribution of the inclusion centroids, and sufficiently fast decay in the usual 'no long-range order' hypothesis, the integral over the complement of $\Omega_d^{(rs)}$ is in fact identically zero. This is shown in Appendix A of the paper by Ponte Castaneda & Willis (1995). Therefore, the expression (B8) for $\langle \mathbf{A}^{(rs)} \rangle$ telescopes down to

$$\langle \mathbf{A}^{(rs)} \rangle = -p^{(r)} p^{(s)} \int_{\Omega^{(r)}} d\mathbf{y} \int_{\Omega^{(s)}} d\mathbf{y}' \int_{\Omega_d^{(rs)}} d\mathbf{z}'' \, \mathbf{G}^{(0)}(\mathbf{y} - \mathbf{y}' - \mathbf{z}'') + \delta_{rs} p^{(r)} \int_{\Omega^{(r)}} d\mathbf{y} \int_{\Omega^{(s)}} d\mathbf{y}' \, \mathbf{G}^{(0)}(\mathbf{y} - \mathbf{y}'). \tag{B10}$$

Since $\mathbf{y} \in \Omega^{(r)}$ and $\mathbf{y}' \in \Omega^{(s)}$ ensures that $\mathbf{y} - \mathbf{y}' = \Omega_d^{(rs)}$, it follows that

$$\int_{\Omega_d^{(rs)}} d\mathbf{z}'' \, \mathbf{G}^{(0)}(\mathbf{y} - \mathbf{y}' - \mathbf{z}'') = \mathbf{G}_d^{(rs),} \tag{B11}$$

which is equal to the constant tensor given in eq. (69). We note that $\mathbf{G}_d^{(rs)} = -\mathbf{P}_d^{(rs)}$, where $\mathbf{P}_d^{(rs)}$ is the spatially invariant tensor given by eq. (3.14) in the paper of Ponte Castaneda & Willis (1995). (We follow the same sign convention for the strain Green's function as Gubernatis & Krumhansl (1975), whilst Ponte Castaneda & Willis (1995) uses the opposite convention.) If we now combine eqs (B10) and (B11), and make use of the fact that $v^{(s)} = |\Omega^{(s)}| p^{(s)}$, than we arrive at the following expression for the averaged geometric parameters:

$$\langle \mathbf{A}^{(rs)} \rangle = \delta_{rs} v^{(r)} \mathbf{G}^{(s)} - v^{(r)} v^{(s)} \mathbf{G}_d^{(rs)}. \tag{B12}$$

APPENDIX C: COMPARISON WITH HUDSON'S CRACK MODEL

The first-order correction in Hudson's (1980) theory agrees with Eshelby's first-order complete expansion (identical to the average t-matrix in our model), provided that the aspect ratio is sufficiently small, and the weak-material (fluid-filled) formulation of Hudson (1981) is used for the former case (see Cheng 1993).

The second-order correction in Hudson's (1980) theory (that was evaluated under the assumption that the spatial distribution of cracks is spherically symmetric) involves a fourth-rank tensor $\{\chi_{ijl}\}$, which is identical to μ times the $\mathbf{G}_d$ tensor in eq. (74), provided that the $\mathbf{G}_d$

tensor is calculated for a spherical inclusion embedded in the matrix (uncracked) material, characterized by an isotropic stiffness tensor $C^{(0)}$, associated with the shear modulus μ.

From the above observations, it is clear that one can easily derive an expression for the *t*-matrix of a single Hudson crack, which can be inserted into the more general *T*-matrix approximation (71)/(73), if the goal is to evaluate the effects of spatial distribution at higher crack densities, without using the (heuristic) perturbation technique of Padé approximants (see Cheng 1993).

For example, if we consider a family of *F* Hudson cracks with normals in the same direction (defining the zonal axis of the effective medium of hexagonal symmetry), we obtain

$$t_{ijkl}^{(r)} = \frac{3}{4\pi\mu\alpha^{(r)}} C_{ij3s}^{(0)} U_{st}^{(r)} C_{t3kl}^{(0)}, \tag{C1}$$

where $\alpha^{(r)}$ $(r = 1, \ldots, F)$ are aspect ratios of the cracks and $\{U_{mn}^{(r)}\} = \text{diag}\{U_{11}^{(r)}, U_{11}^{(r)}, U_{33}^{(r)}\}$, where $U_{11}^{(r)}$ and $U_{33}^{(r)}$ are (the familiar displacement discontinuity parameters) generated by the response of a circular crack to shear and normal stress, respectively. If the cracks are isolated with respect to fluid flow, one can use the expressions for the displacement discontinuity parameters derived by Hudson (1981, 1988) for fully and partially saturated cracks, respectively; if the cracks are no longer isolated with respect to fluid flow see Hudson *et al.* (1996).

The above result was obtained by (setting Hudson's first-order correction equal to $\sum_r v^{(r)} \mathbf{t}^{(r)}$) using the following expression for the volume concentration $v^{(r)}$ of the *r*th set of Hudson cracks:

$$v^{(r)} = \frac{4}{3}\pi\epsilon^{(r)}\alpha^{(r)}. \tag{C2}$$

Here $\epsilon^{(r)} = v^{(r)}(a^{(r)})^3$ is the corresponding crack density, where $v^{(r)}$ is the number of cracks per unit volume and $a^{(r)}$ is the length of the short axis of the spheroidal crack.

If the cracks are no longer fully aligned, the expression (C2) for the *t*-matrix of a typical Hudson crack can still be used, but then in conjunction with suitable coordinate transformation methods (e.g. Jakobsen *et al.* 2002).